Journal of Hydrology: Regional Studies 41 (2022) 101093

Contents lists available at ScienceDirect

Journal of Hydrology: Regional Studies

journal homepage: www.elsevier.com/locate/ejrh

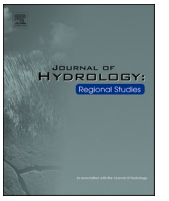

Lake surface area expansion: Insights into the role of volcano-tectonic processes, Lake Beseka, East Africa

Esayas Gebremichael [a,*], Wondwosen M. Seyoum [b], Benite Ishimwe [a], Guzalay Sataer [c]

[a] Department of Geological Sciences, Texas Christian University, 2955 South University Drive, Fort Worth, TX 76109, USA
[b] Department of Geography, Geology and the Environment, Illinois State University, Normal, IL 61790, USA
[c] Geological and Environmental Sciences Department, Western Michigan University, Kalamazoo, MI 49009, USA

ARTICLE INFO

Keywords:
Volcano-tectonic
Lake surface area expansion
InSAR
Beseka

ABSTRACT

Study region: Lake Beseka, Ethiopia
Study focus: Lake Beseka has been expanding despite climatic and other relevant variables remaining largely the same over time. In this study, we applied an integrated approach based on multi-source datasets—Synthetic Aperture Radar (SAR), Landsat thermal band data, precipitation, and physicochemical and isotope water quality data—to understand the processes that govern the lake surface area expansion with a focus on the volcano-tectonic process.
New hydrological insights for the region: Our findings show the following: (1) overall annual rainfall trend showed a declining trend, suggesting that rainfall is not the main source of water that led to the expansion of the lake; (2) recent vertical deformation rates reveal high subsidence rates on areas bordering the lake to the north, west, and southwest that are dissected by an echelon of fissures and faults, and physicochemical and isotopic water quality analysis from previous studies reveal dilution of the lake water by a new source of water in these parts; and (3) the thermal data analysis showed high land surface temperature values to the north of the lake, where a recent swarm of earthquakes were detected. We attributed the lake surface area growth to two processes: groundwater influx into the lake surface facilitated by active volcano-tectonic processes and volcano-tectonic-induced subsidence that creates favorable conditions for the water to expand to new areas.

1. Introduction

Earth's dynamic climate is the most significant factor that controls the size and depth of lakes. Coupled with climatic changes, anthropogenic interventions, including land use and land cover changes, the construction of engineering structures, such as dams and lake water withdrawal, are increasingly playing major roles in controlling the size and water levels of lakes (Kraemer et al., 2020). Several lakes in different parts of the world are undergoing expansion owing principally to the combination of the two factors outlined earlier (Theuerkauf and Braun, 2021). For instance, increasing water level trends have been noted during the years 1992–2019 on several of the world's large lakes, and the change has been attributed to background climate oscillations, such as the El Niño–Southern Oscillation and anthropogenic controls (Kraemer et al., 2020). On the other hand, several other lakes, including endorheic lakes in arid

* Corresponding author.
E-mail address: e.gebremichael@tcu.edu (E. Gebremichael).

https://doi.org/10.1016/j.ejrh.2022.101093
Received 26 January 2022; Received in revised form 30 March 2022; Accepted 18 April 2022
Available online 26 April 2022

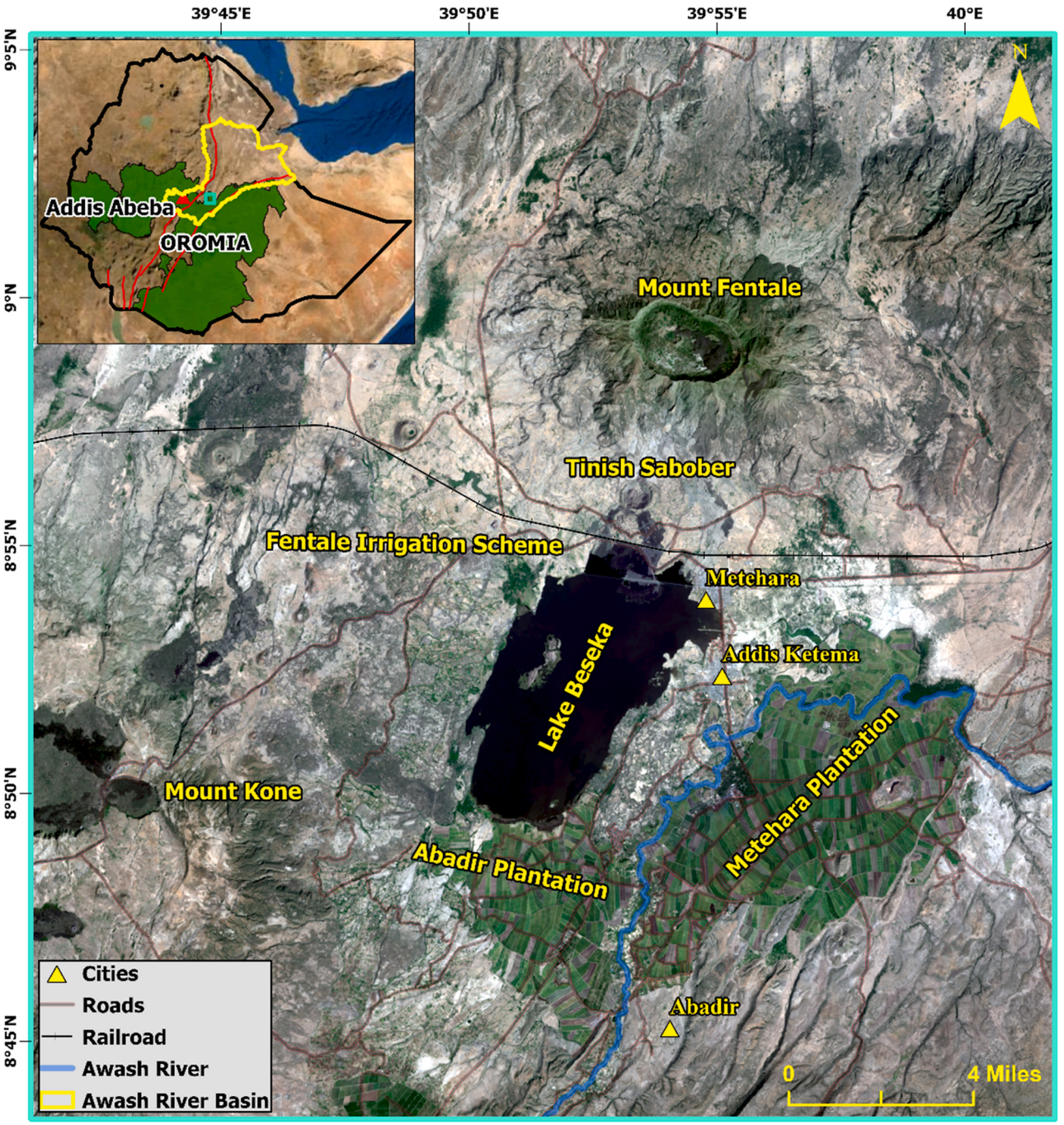

Fig. 1. Location map of the study area. Inset map shows the location of the study area with respect to the federal regional administration structure of Ethiopia (shown in green fill), the rift valley escarpments (shown in red outline), and the Awash basin (shown in yellow outline).

and semi-arid climates, were noted to have experienced severe water loss and level decline in the past few decades mainly due to variations in the long-term climatic conditions and human impact (Busker et al., 2019; Prange et al., 2020; Wang et al., 2018; Wurtsbaugh et al., 2017).

In addition to climatic variables and anthropogenic activities, active volcano-tectonic forcings control the dynamics of lake level, size, and potentially depth of lakes (Abbott and Anderson, 2009; Owen et al., 2019). The role of such processes in altering the dynamics of endorheic lakes can be explained in a twofold process: tectonic structures serving as fluid pathways to transport high-temperature groundwater, formed from active volcanic processes in the subsurface and their interactions with the groundwater, to lake floors (Brehme et al., 2019; Hancock et al., 1999; Kapchenko and Grozdova, 1997). In a similar process but yet in a reverse direction of flow,

tectonic structures and processes may lead to the draining of the lake water to the groundwater system, or seepage to the surface or surface waterbody (Sakai et al., 2016). In addition to constraining the water level dynamics, volcano-tectonic forcings alter the morphology and surface area of the lakes (Talbot, 2005).

One region of the world in which volcano-tectonic processes control the formation and temporal fluctuations in the depth and extent of lakes is the Ethiopian Rift Valley. This region is part of the northern branch of the Great East African System that extends from Mozambique to the Afar triple junction located south of the Red Sea (Acocella et al., 2002). Most of the volcano-tectonic process-controlled lakes found in the Ethiopian Rift Valley are found in the part of the Ethiopian rift system located to the south of the Afar Triangle, called the Main Ethiopian Rift (MER) (Bonini et al., 2005; Gasse and Street, 1978). The MER has been volcanically, tectonically, and seismically active during the Holocene. Most of these processes are spatially concentrated within the Wonji Fault Belt, a region known for intense normal faulting and volcanism related to the Quaternary episodes of extension and characterized by a series of NNE–SSW trending normal faults and fissures of the MER (Chernet et al., 1998; Mohr, 1987; Le Turdu et al., 1999; Williams et al., 2004).

In the northern part of the MER, major rifting and downwarping processes that gave rise to the recent morphology started during the late Miocene (10–11 Ma) and commenced till present day (Bonini et al., 2005). Similar processes in the central and southern parts of the MER began during early Miocene (Chernet et al., 1998; Williams et al., 2004). Extensive tectonic and volcanic activities within the MER have given rise to the accommodation zones that eventually formed several lakes within the region (Alemayehu et al., 2006; Ayenew, 2004).

The morphologies and lake level parameters in most of the lakes in MER are largely constrained by climatic fluctuations and human interventions (Alemayehu et al., 2006; Benvenuti et al., 2002). For example, Lake Abiyata shrunk by half during 1980–2010, which is mainly due to human interventions such as lake water withdrawal and diversion of tributaries and, to a lesser extent, due to drought (Seyoum et al., 2015). On the contrary, few other lakes within the MER have seen an increase or decrease in lake surface area since the past few decades, even though there has been little to no change in climatic variables and human interventions during the times—a trait that has been hypothesized to have occurred due to volcano-tectonic drivers.

Lake Beseka (Fig. 1), an endorheic lake in MER, has considerably expanded over the past few decades (lake surface area in 1972 = 10.8 km^2; 2020 = 52.1 km^2) though climatic and other relevant variables have remained largely the same during the time. The lake level is rising on average annual rates ranging from 0.14 to 0.2 m (Klemperer and Cash, 2007; Goerner et al., 2009; Yimer and Jin, 2020). Even more interesting is the fact that the lake growth and expansion follows an irregular pattern of growth and seems to have experienced accelerated growth in the past two decades (1981: 27.5 km^2; 2001: 38.9 km^2; 2020: 52.1 km^2). The uncontrollable spatial expansion of Lake Beseka has incurred adverse socio-economic and environmental ramifications (Ayenew, 2004; Dinka, 2017, 2020). Due to the saline and alkaline chemical composition of the water, it is neither suitable for drinking nor irrigation purposes (Dinka, 2010), making the impact of the encroachment severe, particularly on plants and crops.

Several studies provided conflicting hypotheses on the causes and mode of evolution of the processes that gave rise to the lake expansion. In some of the proposed hypotheses, neotectonic processes and their influences on the groundwater dynamics, and other processes such as the direct flow from the nearby irrigated agricultural fields, have been credited for the rise. Moreover, change in groundwater dynamics (gradient of flow towards the lake watershed) following the construction of the Koka dam in the neighboring watershed has also been cited as potential sources of water, giving rise to the lake level change and the ensuing expansion (Alemayehu et al., 2006; Ayenew, 2004; Ayenew and Legesse, 2007; Dinka, 2017; Goerner et al., 2009; Jin et al., 2021; Tessema, 1998; Yimer and Jin, 2020). In the previous studies that ascribed neotectonic processes and movements as the fundamental controllers of the lake expansion, the role of vertical surface deformation processes has not been explained, or the effects are stated to be insignificant. Asfaw et al. (2006) applied differential leveling procedures on selected benchmarks surrounding the lake region during two leveling campaigns (July 1995 and November 2003). They stated that tectonic subsidence has little or no effect on the lake level expansion of Lake Beseka. On the other hand, Goerner et al. (2009) calculated a maximum subsidence rate of ~ 1 cm/yr for the Lake Beseka area. This rate was calculated by taking into consideration the average of the spreading velocity estimated for the MER by Bilham et al. (1999) using Global Positioning System (GPS) measurements acquired between 1969 and 1997, and the average of the field dip angle measurements of the faults bordering the lake. They concluded that the impact of subsidence on the lake basin volume change is insignificant but stated that neotectonic activity has altered the groundwater flow pattern and resulted in the formation of a large underground catchment that contributed the lake level rise (Goerner et al., 2009). The spatial limitation of leveling and other geodetic methods limits the ability of the methods to account for the deformation between measurement stations because of the sparse distribution of the permanent or campaign measurement stations. Moreover, potential measurement errors, cost, disturbance/destruction of some of the benchmarks between leveling campaigns (as in the case of Asfaw et al., 2006) as well as the inherent limitation of height measurements from leveling and other geodetic procedures, such as systematic errors and seasonal surface height fluctuations (Lyon et al., 2018), could have affected the outcome of the analysis and hence inaccurate conclusion. In the absence of appropriate datasets and results derived using effective data analysis approaches that indicate local and regional tectonic processes with improved accuracies, it would be difficult to discern active tectonic structures that contribute to the lake level rise from those that are not. In addition to assessing the contribution of tectonic controls on Lake Beseka expansion, the potential role, relevance, and impact of ongoing active volcanic processes in the mountain region neighboring the lake region, as evidenced by the recent swarm of earthquake events (Keir et al., 2006, 2006; Temtime et al., 2020) on the lake surface area expansion, have not been investigated in the earlier studies.

Interferometric Synthetic Aperture Radar (InSAR) technique has proven to be an efficient tool for quantifying vertical surface deformation rates resulting from different processes including volcano-tectonic because of its capability to observe deformation over a large area with sub-centimeter to sub-millimeter accuracy (Burgmann et al., 2000; Chen et al., 2000; Gebremichael et al., 2018; Haley et al., 2022; Hooper et al., 2007; Tantianuparp et al., 2013). Synthetic Aperture Radar (SAR) datasets of varying wavelengths acquired

by side-looking radar instruments that are capable of image acquisition under all-weather and lighting conditions are used as input in the deformation analysis using InSAR techniques (Balzter, 2001; Burgmann et al., 2000). In SAR methods exploit the differences in the phase component of the SAR signal/data acquired at different times from different orbital positions to quantify displacement (Crosetto et al., 2016; Hanssen, 2001; Pepe and Calò, 2017). Several studies have employed different InSAR and other geodetic techniques to successfully quantify deformation rates induced by active volcano-tectonic processes (Chavez Hernandez et al., 2020; Hooper et al., 2007; Poland et al., 2006; Wauthier et al., 2012). As stated earlier, data unavailability between stations due to the spatially sparse distribution of permanent or campaign measurement stations and the different sources of errors lower the reliability of measurements derived using leveling and other geodetic methods. On the other hand, the multi-temporal and synoptic visualization of the surface provided by SAR datasets makes the long-term monitoring of surface deformation processes using the datasets feasible (Gama et al., 2020) in contrast to the other geodetic techniques (Yang et al., 2016). With respect to the study area and the MER region in general, few studies have explored local and regional surface deformation and changes emanating from volcano-tectonic processes that indicate active subsurface processes in the region (Hutchison et al., 2016; Temtime et al., 2020); however, the link between these processes and the observed surface area changes in some of the lakes in the MER was neither established nor explained. To complement the InSAR-derived result, integrating surface deformation parameters with other relevant datasets would be beneficial, thus further strengthening the hypothesis related to the controls of volcano-tectonic processes on the lake level rise and expansion. This would enhance understanding of the magnitude of the role of the subsurface processes. One possible manifestation of active subsurface processes is the variation in the thermal radiation state of the ground (Caputo et al., 2019; Darge et al., 2019; Ma et al., 2010). In addition, the frequency of seismic activities, and the spatial distribution of earthquake epicenters and their depth of occurrence are also indicators of ongoing active volcano-tectonic processes (Barchi et al., 2021; White and McCausland, 2016).

Understanding the mechanisms and processes that trigger the lake level rise and expansion would be beneficial in order to implement appropriate mitigation efforts to lessen the adverse effects. For that reason, a comprehensive study that provides a holistic view of the processes and factors that contribute to the lake level rise and expansion is imperative. This will assist in resolving the observed discrepancies, such as the observed irregular pattern of the lake surface area growth over time, as well as assess the potential role of volcano-tectonic processes in constraining the expansion. In this study, we accomplish the following tasks (1) decipher the processes and factors that contributed to the intense lake surface area expansion over the course of four decades; (2) quantify the rates of the different processes, such as surface deformation rates, that potentially could contribute to the lake surface area growth; and (3) analyze the directions of the future lake surface area growth and assess the impact on communities, resources, infrastructure, and the ecosystem.

1.1. Geologic, hydrologic, and climatic settings

The area under investigation in this study is Lake Beseka and its immediate surrounding region (area: 1519 km^2; Fig. 1). It is located at the boundary between the MER and the Afar triangle of the Ethiopian rift system. It encompasses Lake Beseka, Awash River, Mount Fentale – a rhyolitic stratovolcano with a summit caldera (Fubelli and Dramis, 2015; Williams et al., 2004), Tinish Sabober – a basaltic tuff cone (Williams et al., 2004), irrigated plantations (Fentale, Metehara, and Abadir located to the northwest, east, and south, of Lake Beseka, respectively), and two major cities (Metehara and Addis Ketema) (Fig. 1). Mount Fentale is the northern end of the MER and marks the transition from the MER to the Afar Triangle (Acocella et al., 2011; Fig. 1). Though the last eruption of Mount Fentale was in the early 19th century, it is believed that the Mount Fentale area is considered an active system owing to the observed ongoing release of volcanic gases, recurrent seismic activity, and historical fissural basalt flows as recent as 1810 that signify potentially active subsurface processes (Asfaw, 1982; Belay, 2009; Harris, 1844; Hunt et al., 2017; Keir et al., 2006, 2006; Temtime et al., 2020; Williams et al., 2004).

The geology of part of the study area surrounding the lake is comprised of volcanic rocks, mainly recent to sub-recent basalts, ignimbrite, rhyolite, and tuff. The floor and edges of Lake Beseka are constituted by Pleistocene lacustrine sediments. Clayey and silty alluvial deposits dominate the irrigated plantations that are neighboring the southern and eastern parts of the lake (EIGS, 1978; Kebede, 1987; Williams et al., 2004). The area is dissected by a dense network of NNE–SSW trending faults and fissures belonging to the Wonji Fault Belt (Berhe, 2007). The lake water body lies in a 5–6 km-wide graben bounded by NNE–SSW trending faults. While extensional normal faults make up the majority of the tectonic structures of the study area, a small number of fissures also exist, particularly in the area that lies between Lake Beseka and the Fentale caldera (Alemayehu et al., 2006; Asfaw et al., 2006; Williams et al., 2004) (Fig. 1).

The study area is located within the Awash River Basin (drainage area: 116,375 km^2), one of the largest basins in Ethiopia comprising major water bodies, including Awash River, Koka water reservoir, and Lake Beseka. The rainfall and temperature patterns of the area indicate a semi-arid climatic condition in which evaporation exceeds precipitation in almost all of the months in a year (Dinka, 2012; Goerner et al., 2009). Two wet seasons (July–September; March–April) supply the area with rainfall (Belay, 2009). The watershed that comprises Lake Beseka, 480 km^2 in area, is oriented in NNE–SSW direction indicating the influence of the regional tectonic structures on the morphology of the watershed (Belay, 2009). The northeastern boundary of the watershed that encompasses the lake region borders the western sides of the Mount Fentale crater (Fig. 2). A segment of the Awash River flows through the study area and is the main source of water for the irrigated plantations. The surface water flow direction in the watershed follows the elevation gradient and is directed towards the lake (Fig. 2).

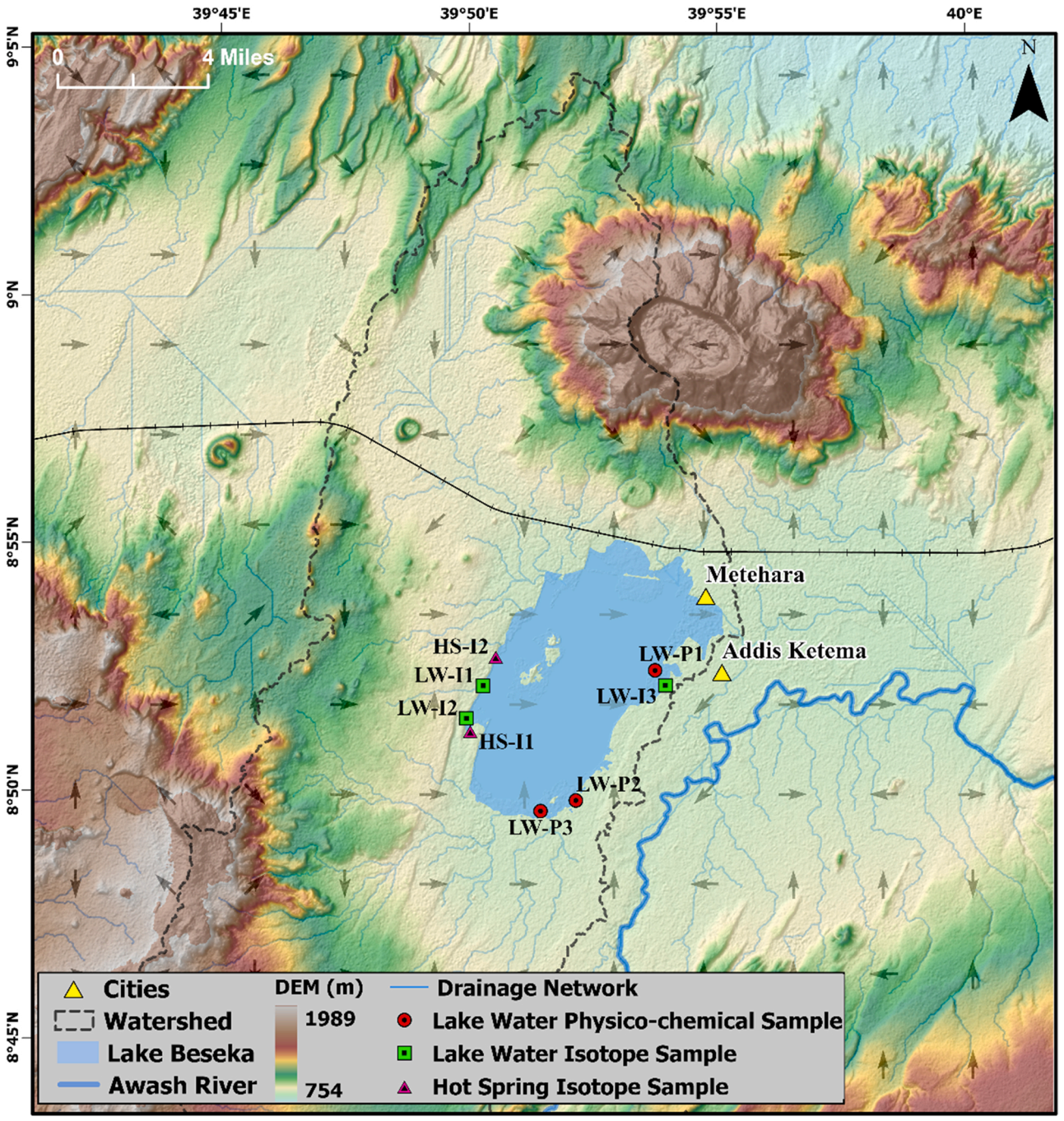

Fig. 2. General hydrology of the study area. Grey arrows indicate flow direction. Lake water sampling sites for physicochemical and isotope analysis are shown as LW-P and LW-I, respectively, while sampling sites for the isotopic analysis of water from hot springs are shown as HS-I (after Belay, 2009; Goerner et al., 2009; Ministry of Water, Irrigation and Electricity (MWIE), 2015).

2. Data and methods

We applied an integrated approach that is based on multi-source datasets, including hydrological, thermal and radar satellite observations, and relevant datasets (e.g., fault, seismic datasets) to analyze the causes of lake surface area growth, quantify the rates of processes that indirectly or directly contribute to the lake growth, and analyze future lake expansion trends as outlined in the study objectives. The datasets and analysis results were evaluated in a Geographic Information Systems (GIS) environment in search of spatial relationships and interactions between the various datasets and analyses results that represent different processes. Through the spatial analysis, we also demonstrated the potential roles (or not), whether direct or indirect, of different variables credited for the lake

level rise and expansion in the earlier studies.

2.1. Hydrology

2.1.1. Precipitation and watershed delineation

Long term (from January 1981 to December 2019) monthly rainfall data were obtained from the Climate Hazards Center InfraRed Precipitation with Station data (CHIRPS) (Funk et al., 2015) were used to see if rainfall has contributed to the expansion of the lake (Funk et al., 2015). The CHIRPS 2.0 data with a 0.05-degree resolution was aggregated to the study area and used to calculate seasonal and annual rainfall. The limited number of rain gauge stations and their uneven spatial distribution coupled with the inconsistency of the data in terms of limited span and/or missing data (Mulugeta et al., 2019) has made the CHIRPS data the optimum data source to analyze long-term precipitation patterns in this study. CHIRPS data are excellent for seasonal drought monitoring and trend analysis (Funk et al., 2014). To investigate the seasonal trend, the months of a year were divided into four seasons: January–March (JFM), April–June (AMJ), the rainy season July–September (JAS), and the dry season October–December (OND). Both Mann–Kendall test (Kendall, 1975; Mann, 1945) and Sen's slope estimator (Sen, 1968) were applied to determine the presence and magnitude of trends on the seasonal and annual rainfall data.

For delineating watershed and extracting the stream networks, a 12.5 m spatial resolution digital elevation model (DEM) acquired by the Phased Array type L-band Synthetic Aperture Radar (PALSAR) sensor on board of the Advanced Land Observing Satellite (ALOS-1), was used. The ArcGIS hydrology tool was adopted to generate watershed boundary and stream network products, and to define flow directions for the surface runoff.

2.1.2. Water quality

In situ physicochemical (Belay, 2009; Dinka, 2017; Goerner et al., 2009; Kebede et al., 1994) and isotopic (Ayenew et al., 2008; Bretzler et al., 2011; Kebede et al., 2008; MWIE, 2015) groundwater and surface water quality datasets from earlier studies were mapped and their spatial relationship with the other parameters were analyzed in a GIS setting (Fig. 2). The physicochemical parameters in consideration were pH, electrical conductivity (EC) given in μs/cm, and major cations (Na^{+}, K^{+}, Ca^{2+}, and Mg^{2+}) and anions (HCO_3^{-}) given in parts per million (ppm). For the stable isotopes, concentrations of the stable isotopes of hydrogen (^{2}H) and oxygen (^{18}O), expressed in parts per thousand (‰), were evaluated to investigate the spatial and temporal variation in concentrations, and the possible interaction of waterbodies within the study area that could contribute to the lake expansion. Though the quality and accuracy of such point measurements, as explained in the case with ground-based geodetic measurements (Section 1), are affected by data gaps between sampling points, they nonetheless provide a general overview of the spatial variation of the parameters across various parts of the lake.

2.2. Surface deformation processes and future lake expansion model

2.2.1. Surface deformation data

We used two sets of SAR datasets acquired during different time frames within the past nearly two decades for quantifying surface deformation processes that would indicate active surface and subsurface processes and their influences on the lake surface area change, and also to evaluate the progressive change in deformation to assess the stability or otherwise of the deformation signal in space and time. Analysis of the latter could account for the observed varying rates of lake surface area expansions. The first set of SAR datasets used in this study were acquired by the Environmental Satellite (Envisat). The now defunct satellite was operated by the European Space Agency (ESA) and delivered C-band (5.6 cm wavelength) SAR data until 2012 (Bartsch et al., 2016; Kucharski et al., 2014). We

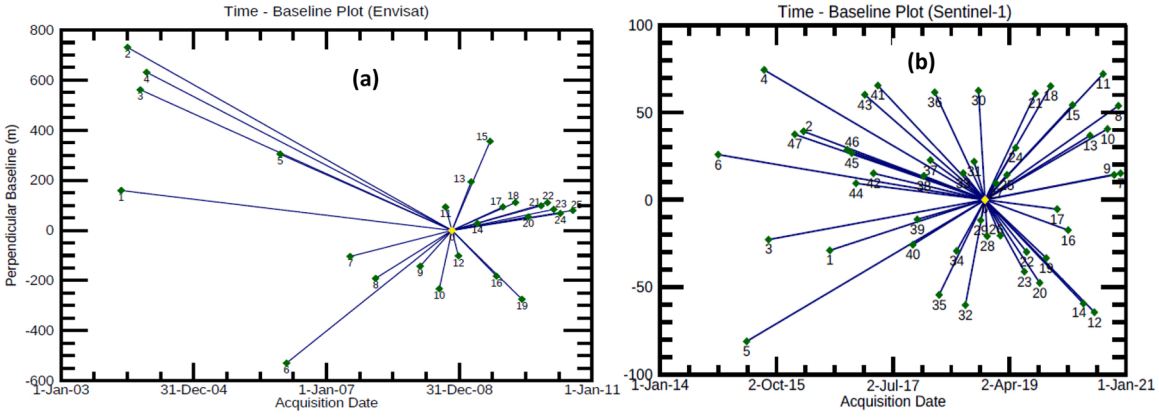

Fig. 3. Baseline time plot for Envisat SAR data (a) and Sentinel-1 (b). The reference images (shown in yellow color) for the Envisat stack and Sentinel-1 stack were obtained on 21 November 2008 and 19 November 2018, respectively, while the maximum perpendicular baseline values for the Envisat and Sentinel-1 stacks were 730.57 m and 74.36 m, respectively.

used 26 descending Envisat SAR Single Look Complex (SLC) level data acquired between the interval 2003–2010 (Fig. 3a) along track 49 to estimate the deformation rate over the investigated interval. The second set of C-band SAR datasets used in this study were acquired by the Sentinel-1 mission. The Sentinel-1 is a C-band SAR constellation, operated by the ESA, capable of providing SAR imaging of the globe with short revisit times ranging from 6 to 12 days (Barra et al., 2017). We used 48 descending Interferometric Wide (IW) swath mode Sentinel-1 SLC SAR imagery acquired along path/track 79 and frames 561 and 563 and spanning from 2014 to 2021 (Fig. 3b) to quantify the deformation rate during the investigated interval. The deformation results derived from the analysis of the two datasets (Envisat and Sentinel-1) were corresponded to one another to assess the progressive change in the deformation signal and to observe whether there was continuity or inconsistency in the deformation signal. Obtaining such information would be crucial to understanding the effect of continuous or changing deformation rates on the lake expansion rates.

2.2.2. Surface deformation method: Persistent Scatterer Interferometry

For quantifying the deformation rates, a subclass of the InSAR analysis method called the Persistent Scatterer Interferometry (PSI) was applied on the two sets of SAR datasets (Fig. 3). This method relies on the deformation analysis of targets/pixels that exhibit strong and consistent scattering properties over time when viewed from different angles, called persistent scatterers (PS) (Hooper et al., 2004, 2012; Jia and Liu, 2016). Using PS targets for determining displacement helps counterbalance the phase noise and decorrelation effect introduced on the InSAR analysis when using distributed scatterers (Zebker and Villasenor, 1992). The PSI method operates by stacking a series of interferograms generated by comparing each one of the SAR images (called secondary images) against a single image (called a reference image) (Fig. 3) (Hooper et al., 2012).

We used the Stanford Method for Persistent Scatterers (StaMPS) software package (Hooper et al., 2004, 2007) for deriving vertical surface deformation rates from the Envisat and Sentinel-1 datasets (Fig. 3). For the Envisat dataset, the steps preceding the final displacement estimation (pre-processing) in StaMPS were facilitated through the Delft object-oriented radar interferometric software (DORIS) package (Hooper et al., 2007; Kampes and Usai, 1999). In the case of the Sentinel-1 dataset, ESA's Sentinel Application Platform (SNAP) software was used to pre-process the SLC images (Foumelis et al., 2018; Zuhlke et al., 2015). Key data processing steps in the StaMPS workflow (including the pre-processing steps in DORIS and SNAP) include (Foumelis et al., 2018; Hooper et al., 2004, 2007; Latip et al., 2015; Sousa et al., 2010):

- Calculating the offset between the images and resampling the secondary images to the coordinate system of the reference image, with the objective of aligning the secondary images with respect to the reference image for determining the phase difference of the same area – a process called coregistration. In the case of Sentinel-1, this step is preceded by the splitting of each of the subswaths of Sentinel-1 IW products followed by the updating of their orbital information.
- An interferogram formation step that also includes the removal of the topographic phase using the Shuttle Radar Topography Mission 1″ (30 m) DEM. For Sentinel-1, debursting and merge procedures are implemented at this stage to seamlessly join the bursts and subswaths respectively.

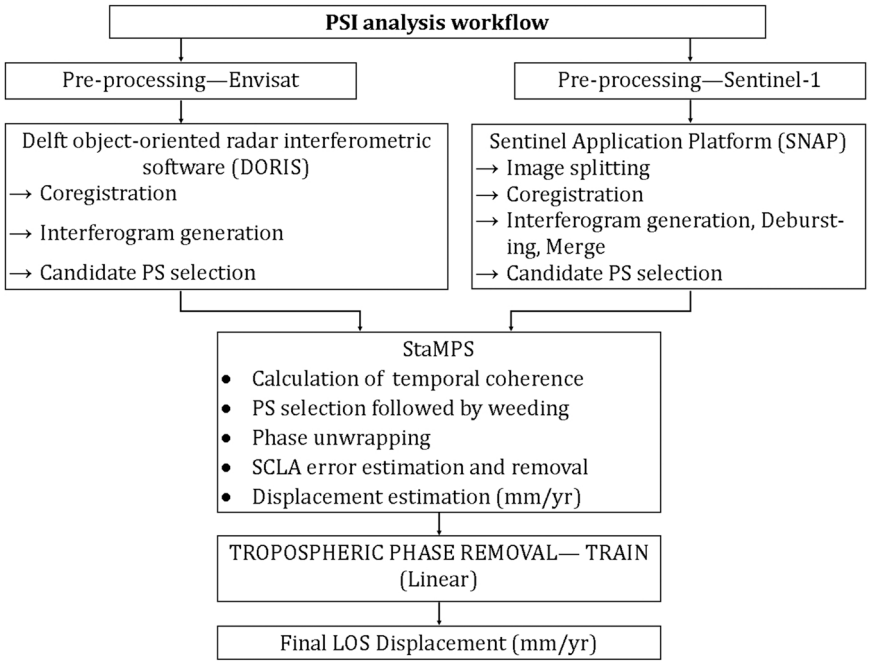

Fig. 4. A simplified flowchart depicting the principal PSI processing steps.

- A PS selection step that is based on a combination of the amplitude dispersion index value and the temporal coherence, which are measures of amplitude and phase stability of the PS, respectively.
- A line-of-sight (LOS) displacement (timeseries) estimation step that follows a phase unwrapping procedure achieved using the Statistical Cost Network Flow Algorithm for Phase Unwrapping (SNAPHU) package (Chen and Zebker, 2001; Hooper, 2010), and the removal of spatially correlated look angle (SCLA) error.

The tropospheric phase contribution on the deformation signal was estimated and removed from the final displacement estimate using the linear approach of the Toolbox for Reducing Atmospheric InSAR Noise (TRAIN) algorithm (Bekaert et al., 2015). A simplified schematic diagram demonstration of the main processing steps is shown in Fig. 4.

2.2.3. Future lake surface area expansion trends

Vertical surface displacement rates, elevation, and surface water flow direction data derived from the DEM (Fig. 2) were integrated to generate a hypothetical probabilistic future change scenario of the lake surface area and point out the direction/s of expansion. In combination with socio-economic and relevant datasets, the impacts of future expansion on the communities and their livelihoods, infrastructure, and the ecosystem were also investigated.

2.3. Land surface temperature

Long-term (1986–2020) spatio-temporal trends in land surface temperature (LST) values that serve as a measure of the variation in the thermal radiation state of the ground over the study area, given in degree Celsius (^{o}C) units, were derived from the analyses of the thermal bands of Landsat 5 (band 6), Landsat 7 (band 6), and Landsat 8 (bands 10 and 11) missions (Table 1) (United States Geological Survey (USGS), 2020). Imagery acquired during the dry season (October–December), where there is little or no cloud cover on the imagery and the influence of precipitation on LST is minimal, were used for generating the LST products. The USGS provides 30-m spatial resolution Landsat thermal datasets after applying the cubic convolution resampling method on the original coarse resolution datasets (Sekertekin and Bonafoni, 2020). LST result generation was based on the workflow described by Parastatidis et al. (2017) and facilitated through a cloud-based platform (Parastatidis et al., 2017). The web platform utilizes the Google Earth Engine product catalog to retrieve Landsat radiance and brightness temperature image collections for the investigated area and date range, and uses the single channel algorithm (Jimenez-Munoz et al., 2009) to calculate LST. For more accurate estimates of LST, land cover emissivity values resulting from the Normalized Difference Vegetation Index (NDVI) estimates were integrated in the analysis workflow (Parastatidis et al., 2017). Analysis to calculate the mean annual LST values for the investigated interval was carried out in a GIS setting.

3. Results

3.1. Precipitation

The overall annual rainfall trend for the interval 1981–2019 for the study area showed a declining trend (Fig. 5) though the trend varies seasonally. During this interval, the lake grew by more than 24 km^2.

Except for one of the dry seasons, JFM, no statistically significant rainfall trend was observed in the seasonal rainfall data (Table 2). During the dry season, the rainfall trend showed a declining trend at a rate of 2 mm per year between 1981 and 2019 (Fig. 6a). The two main rainy seasons, summer (JAS) and spring (AMJ) (Belay, 2009; Yimer and Jin, 2020), showed no statistically significant trend (Table 2, Figs. 6b and 6c); these are the seasons where potential recharge to the lake can occur. The long-term rainfall trend in the dry season (OND) exhibited a decline, though the amount is statistically insignificant (Fig. 6d). The annual rainfall data showed a statistically significant decreasing (3 mm per year) trend. The overall decreasing trend in the annual rainfall (Fig. 5) is due to the declining rainfall during the dry seasons (JFM) (Fig. 6a). Given the annual average rainfall of 600–700 mm in the region, the trends are not significant enough to cause the uncontrollable change in the Lake Beseka.

3.2. Surface deformation

The calculated vertical deformation results (Figs. 7a and 7b) indicate maximum subsidence rates of up to − 6.1 mm/yr and − 5.6 mm/yr for the Envisat (2003–2010) and Sentinel-1 (2014–2020) datasets, respectively. On the other hand, the uplift rates range from + 7 mm/yr and + 6.6 mm/yr for Envisat and Sentinel-1 datasets, respectively. The deformation signal is largely stable/continuous in space and time during the investigated interval, as can be seen in Fig. 7. For example, the calculated deformation rates near a section on the northwestern part of the lake (shown in black-outlined box in Fig. 7(a and b)) show consistency in the

Table 1
The Landsat thermal band data used with the study's investigated intervals.

Mission	Used Thermal Band	Investigated Interval
Landsat 5	Band 6	1986–2012
Landsat 7	Band 6	1999–2020
Landsat 8	Band 10	2013–2020

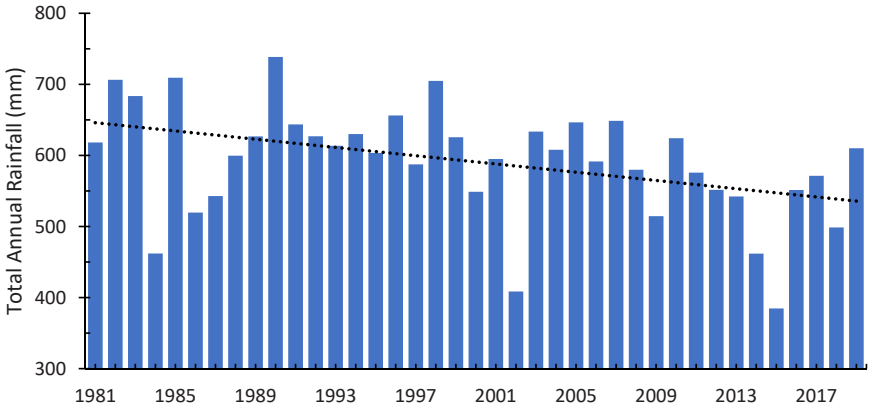

Fig. 5. Annual rainfall trend (1981–2019) of the study area.

Table 2
Mann–Kendall and Sen's slope test results with alpha level 0.05 (p-values in bold are not statistically significant).

	Sample size	Sen slope	Kendall's S	p-value
JFM	39	-2.07	-229	0.01
AMJ	39	-0.28	-37	**0.66**
JAS	39	-0.76	-61	**0.47**
OND	39	0.09	31	**0.72**
Annual	39	-3.00	-241	0.00

deformation signal estimated using both datasets: Envisat (mean deformation: −0.64 mm/yr; standard deviation: 0.69 mm/yr) and Sentinel-1 (mean deformation: −0.58 mm/yr; 0.58 mm/yr) (Figs. 7c and 7d). As seen on the overlapping histograms in Fig. 7c, the PS density for the investigated area (black-outlined box in Figs. 7a and 7b) is higher in the case of Sentinel-1 (2629 PS) compared to Envisat (1140 PS). The collective impacts of longer revisit times (35 days for Envisat while 6–12 days for Sentinel-1) and longer spatial baselines (Fig. 3) may have contributed to temporal decorrelation that ultimately led to lower PS density for Envisat-based PSI analysis (Fiaschi et al., 2019). In addition to the effects of temporal decorrelation resulting from a loss of coherence, the slight difference in the mean deformation rates obtained using the two sets of datasets could stem from remnants of the atmospheric effects even though

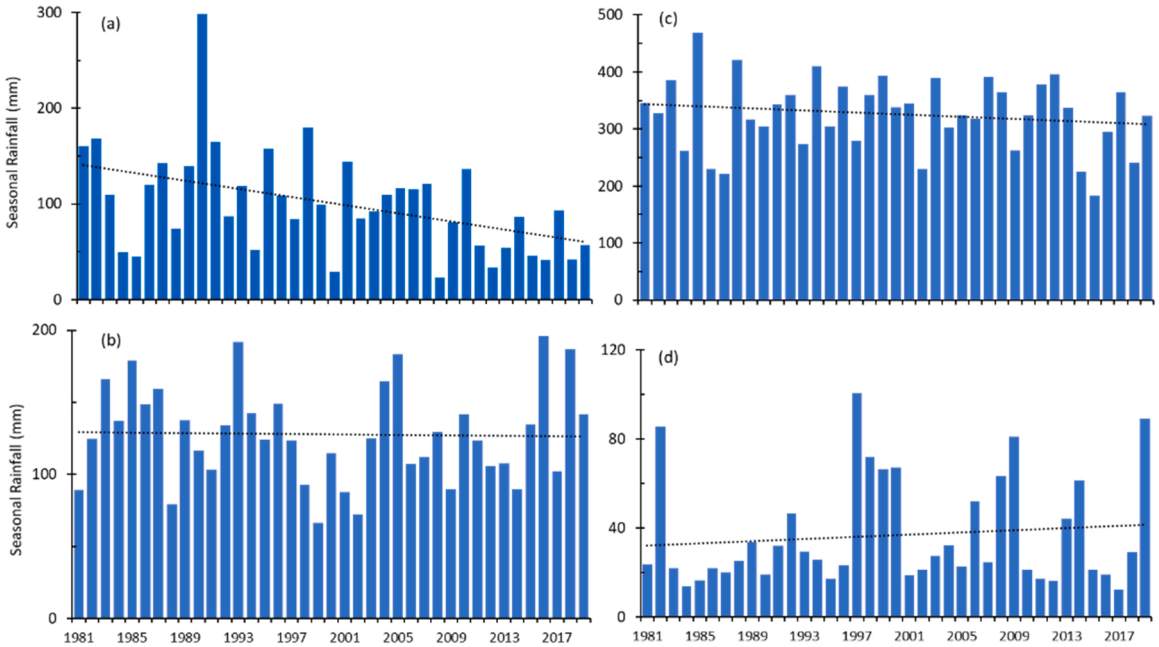

Fig. 6. Seasonal rainfall for the four seasons: (a) JFM, (b) AMJ, (c) JAS (main rainy season), and (d) OND (dry season).

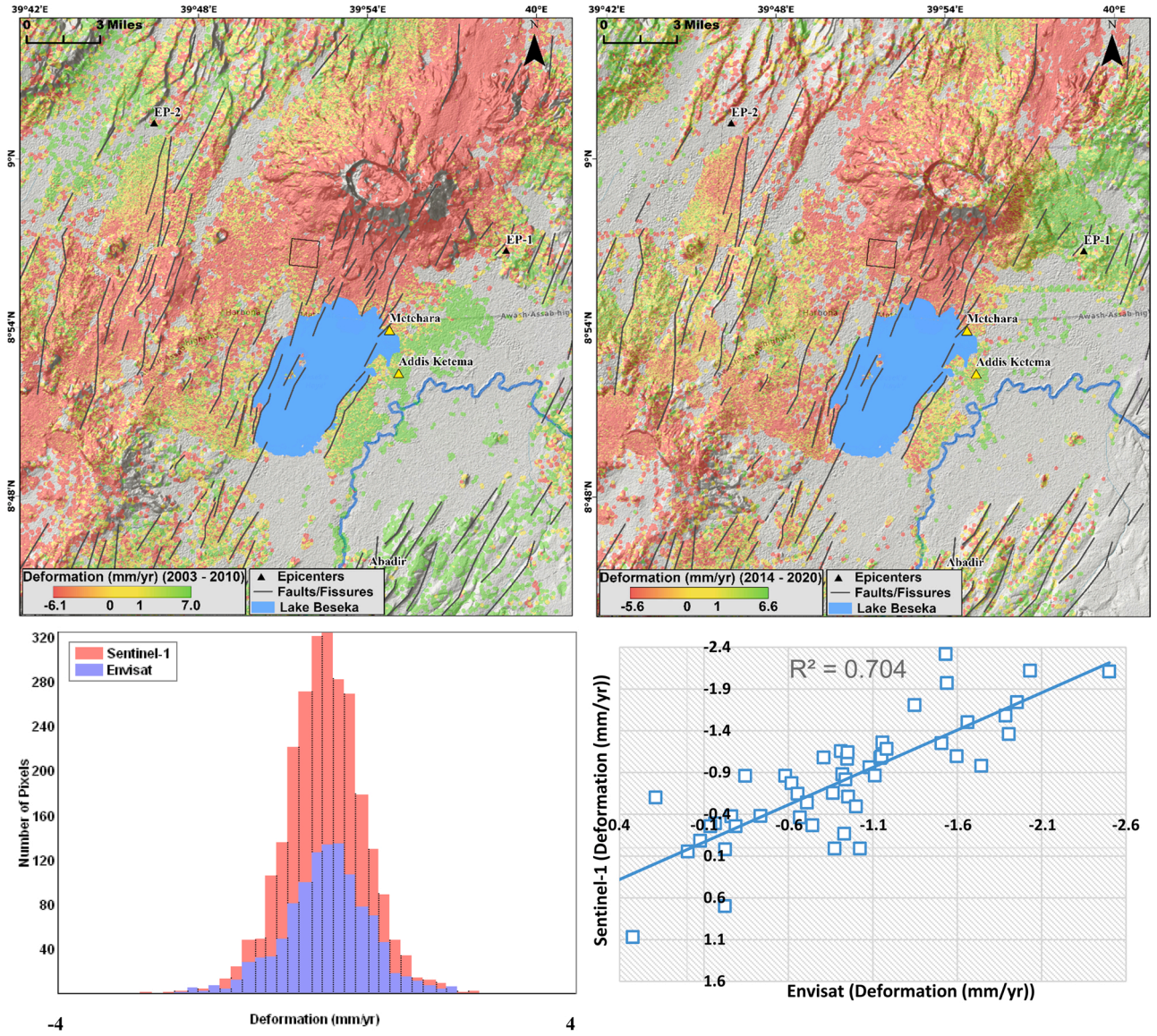

Fig. 7. Deformation estimate (in mm/yr) derived using 26 Envisat SAR (2003–2010) (a) and 48 Sentinel-1 SAR (2014–2020) datasets (b). Shown also are the epicenters of earthquake events that occurred in 1989 and 2015 (EP-1) and 2015 (EP-2) (Hayes et al., 2014; Temtime et al., 2020; USGS Earthquake Catalog (https://earthquake.usgs.gov/earthquakes/search/)). The tectonic structures (faults and fissures (mostly located at the foothills of Mount Fentale)) are shown by the black solid lines (after Belay, 2009; MWIE, 2015; Williams et al., 2004). The black-outlined box (explained in Section 3.2) indicates a sample site chosen to demonstrate the continuity of the deformation signal in time (between Envisat and Sentinel-1 based results). The frequency of the deformation values (c) and the correlation between the displacement rates of PS pixels from both sets of datasets that are within a maximum distance of 20 m (d), are also shown.

atmospheric corrections were applied. It could also be due to changing surface and subsurface processes over time and their influences on the deformation process. The correlation coefficient calculated based on a sample of 50 PS pixels identified on both sets of datasets that are within a maximum distance of 20 m to each other (Fig. 7d) reveals a high correlation value ($R^2 = 0.70$).

Based on recent deformation rates derived from the Sentinel-1 mission (Fig. 7b), high subsidence rates (up to −4.52 mm/yr) were noted on the southern side of Mount Fentale and in the Tinish Sabober cone area located north of the lake (see Fig. 1 for location). This area is dominated by an echelon of parallel to sub-parallel NNW–SSE trending fissures and faults. The summit caldera of Mount Fentale also exhibited a high subsidence rate (up to −4.4 mm/yr) and moderate rates of uplift (3.6 mm/yr) (Fig. 7b). However, the Envisat data-based rates only showed subsidence with rates up to − 6.1 mm/yr in this area (Fig. 7a). Moderate rates of subsidence were calculated for the area near the northwestern (up to −2.3 mm/yr), western (up to −2.5 mm/yr), and southwestern (up to −2.9 mm/yr) edges of the lake that are bounded by a series of NNW–SSW trending faults (Fig. 7b). Moderate rates (up to −3.24 mm/yr) were also calculated for the northeastern edge of the lake area that includes Metehara City (Fig. 7b). Lower rates of subsidence (up to −1. 4 mm/

yr) to near stable deformation rates were calculated for areas bordering the eastern and southeastern parts of the lake. Addis Ketema city is located within about a 1 km distance from the current eastern periphery of the lake (see Fig. 1 for location) and is experiencing a subsidence rate as high as − 2.09 mm/yr (Fig. 7b).

Most of the high uplift rate estimates (up to 5.8 mm/yr) are spatially concentrated to the east and northeast of the lake - near the foothills of the Mount Fentale and surrounding area as clearly shown in Fig. 7b. Higher deformation rates (up to 7 mm/yr) were also calculated for this part of the study area using the Envisat SAR data (Fig. 7a). Similar observations of uplift process to the east and northeast of the lake were also made by Asfaw et al. (2006). This region has recurrently experienced micro to light magnitude (up to 4.9) earthquakes with shallow (~ 10 km) hypocenter (Asfaw, 1982; Belay, 2009; Harris, 1844; Keir et al., 2006, 2006; Temtime et al., 2020). A seismic swarm activity was noted in 2015 on this part of the study area (EP-1 on Figs. 7a and 7b) that was determined to be initiated by a 6 km-long dike intrusion to the north of Mount Fentale and this event led to the formation of cracks and fissures as well as affecting the surface deformation rates (Temtime et al., 2020). The spatial distributions of the major recent (1989–2015) earthquake epicenters (EP-1 and EP-2) are shown in Figs. 7 and 7b.

3.3. Land surface temperature

The thermal analysis results (Fig. 8) indicated a general pattern of high mean annual LST values (up to more than 42.4 °C) around the foothills of Mount Fentale and Tinish Sabober areas located north of the lake (see Fig. 1 for location). Pockets of high LST values (mean LST: ~ 42.6 °C) were also observed near the western and northwestern edges of the lake (Fig. 9). The irrigated plantations (see Fig. 1 for location) (mean LST: ~ 21.5 °C) and the area near the southern and eastern edges of the lake (mean LST: ~ 32.8 °C) exhibited

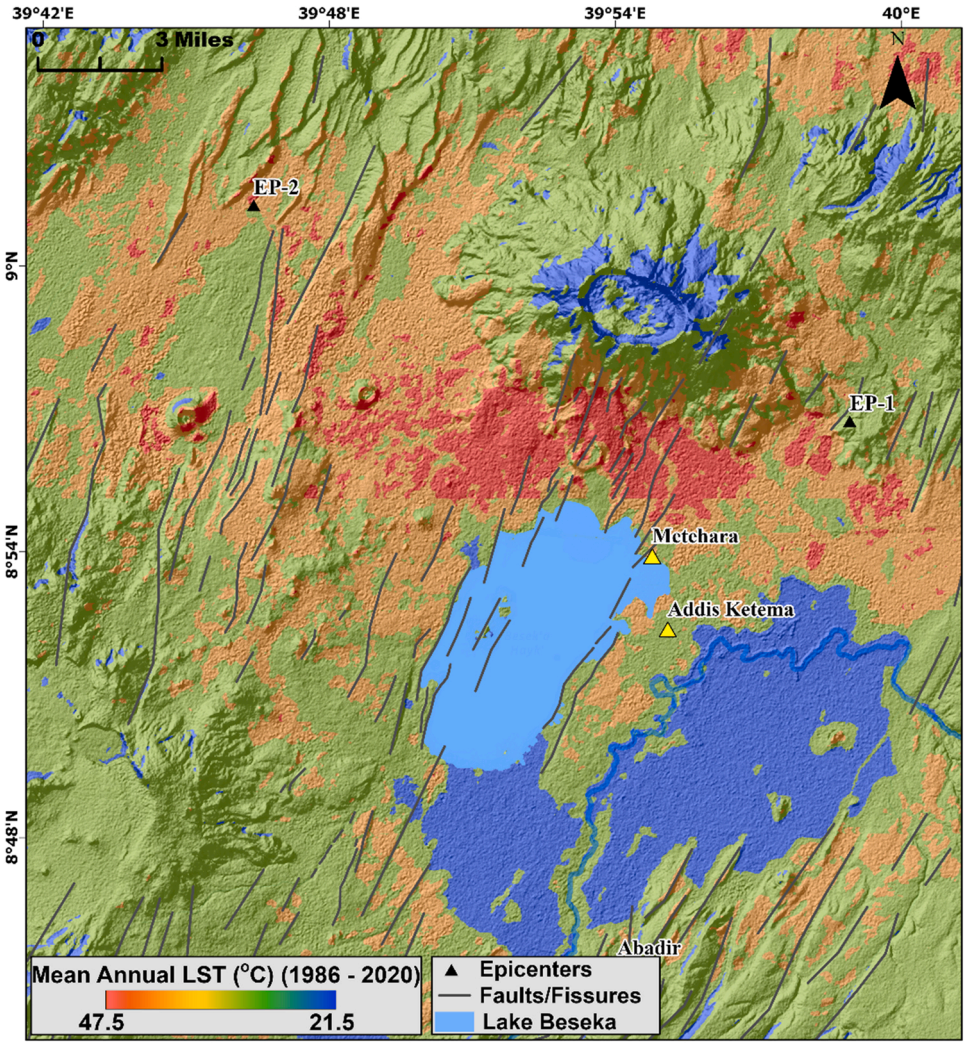

Fig. 8. Long-term (1986–2020) mean annual LST (in °C) of the study area derived from the analyses of the thermal bands of Landsat 5, Landsat 7, and Landsat 8 missions (details shown in Table 1).

low to moderate LST values (Fig. 9).

3.4. Water quality

The concentrations of some of the key physicochemical water quality parameters obtained from Lake Beseka and nearby water bodies have shown changes in recent years (Dinka, 2017). For example, the EC parameter values of water samples obtained from the lake decreased from 7440 μS/cm in 1991–6150 μS/cm in 2015 (sourced from a sampling excursion) (Dinka, 2017; Kebede et al., 1994). During the same interval, the concentrations of K^+, Ca^{2+}, and Mg^{2+} have largely remained the same or had insignificant change in concentration. On the contrary, the concentrations of Na^+ increased from 1810 ppm in 1991 to 2587 ppm in 2015 (Dinka, 2017; Kebede et al., 1994). The change in water quality parameters through time is not consistent spatially throughout the lake. For example, Goerner et al. (2009) demonstrated that samples obtained from the eastern and southeastern parts of the lake (samples LW-P1, LW-P2, and LW-P3; shown in Fig. 2) exhibited a nearly similar EC (~ 6500 μS/cm) and pH values (~ 9.5) while samples acquired near a hot spring on the western escarpment (near HS-I1 in Fig. 2) showed a much lower EC (~ 1650 μS/cm) and pH (8.4) values. Similar observations were also made by Belay (2009). The water type in the western part of the lake, the Na-HCO3 type, is similar to the water type of groundwaters from the rift floor (Belay, 2009; Bretzler et al., 2011; Kebede et al., 2008). Bretzler et al. (2011) observed a high HCO_3 and Na^+ concentration and a near complete removal of Ca^{2+} and Mg^{2+} on water samples from hot springs in fault zones and active volcanic centers, such as the Mount Fentale area. They suggested that a possible combination of a number of processes, such as a hydrolysis reaction that was aided by high CO_2 partial pressures as a result of high CO_2 input from deeper sources, cation exchange, and deep circulation of water that led to the precipitation of Ca^{2+} from hydrothermal alteration processes, contributed to the high concentration (Bretzler et al., 2011). The assessment pertaining to the spatial variability of water quality parameters is further supported with the analysis of the stable isotopes of oxygen and hydrogen on water samples obtained from different parts of the lake and from water bodies surrounding the lake. The long-term precipitation isotopic record of Addis Ababa city was used to establish the local meteoric waterline that is used as a reference to observe the isotopic parameter changes in space and per water source in the study area (Belay, 2009; Kebede et al., 2008; MWIE, 2015).

As is the case for most tropical endorheic lakes in semi-arid to arid climatic zones, Lake Beseka is enriched in δ^2H and $\delta^{18}O$ because of evaporative enrichment (Belay, 2009; Vallet-Coulomb et al., 2008). Similar to the spatial disparity in the concentration values of the physicochemical parameters, the relative enrichment also varies spatially across the lake. The analysis of the stable isotopes of hydrogen and oxygen of water samples acquired on the western and southwestern edges of the lake (samples LW-I1 and LW-I2; shown in Fig. 2) show a relative depletion of the isotopes (δ^2H: 9.79–16.41‰ and $\delta^{18}O$: 1.04–2.69‰) compared with samples (e.g., LW-I3 shown in Fig. 2) retrieved from the eastern part of the lake (δ^2H: 25.77‰ and $\delta^{18}O$: 4.55‰)). Two springs (sample sites HS-I1 and

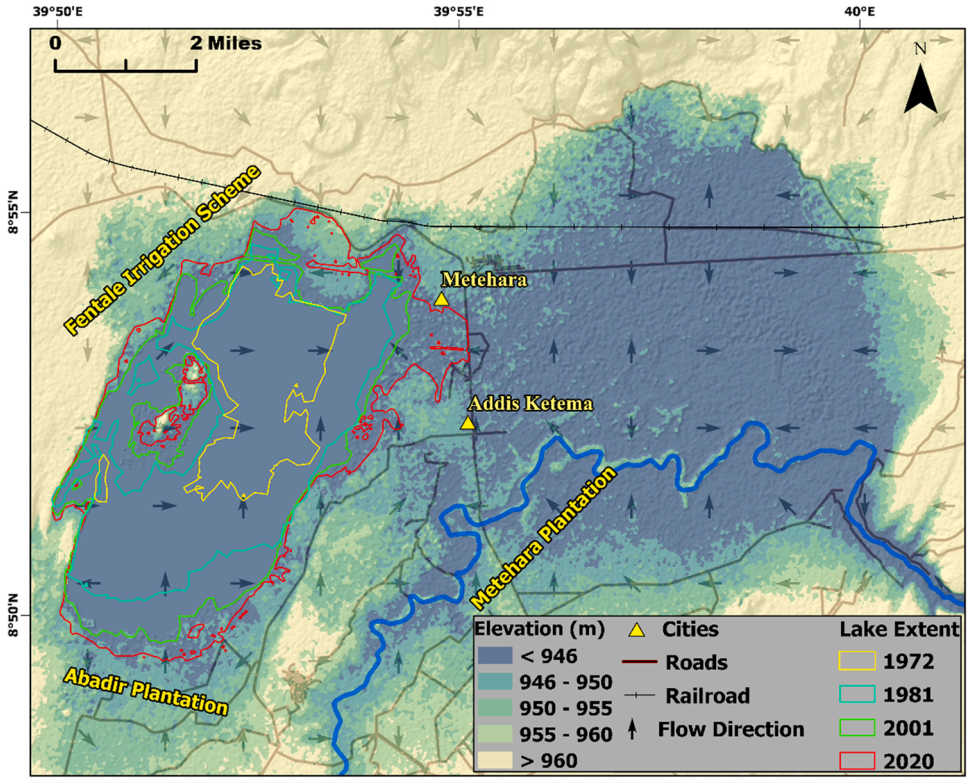

Fig. 9. Future lake surface area growth scenarios and potential effects on infrastructure and agricultural resources.

HS-I2; shown in Fig. 2) that are located proximal to the two samples on the western edge of the lake (samples LW-I1 and LW-I2; shown in Fig. 2) exhibit depletion of both in δ^2H and $\delta^{18}O$: − 9.55–2.55‰ and − 1.74–1.04‰, respectively (MWIE, 2015). The isotopic composition of the groundwater samples from the western and southwestern parts of the watershed that lake Beseka belongs to also shows relative depletion of both δ^2H and $\delta^{18}O$ in contrast to observations east of Lake Beseka (Belay, 2009; Kebede et al., 2008).

4. Discussion

As outlined above, in the absence of significant climatic and meteorological changes (Section 3.1; Figs. 5 and 6), it is conceivable that the lake surface area expansion is caused by other sources, factors and processes. Thus, the climatic factor as a cause for the expansion of the lake is excluded. Since the climate of the study area is semi-arid with low annual precipitation that is not favorable for an agriculture-dependent livelihood, the population density data, which is an indirect indicator of land use and land cover (LULC) change, has not shown significant change over time. For example, from 2000 to 2020, the study area showed a lower population density change of + 21.44 people per square kilometers (Center for International Earth Science Information Network CIESIN, 2018) compared with the national average change of + 35.58 people per square kilometers during the same interval (World Bank, 2021). An analysis of the LULC change of the study area derived using Landsat data for the period 1973–2015 also revealed insignificant change (Dershaye, 2017). This suggests that the influence of LULC change that could result in increased runoff to the lake, even though rainfall trends have shown a decline over the past four decades, is minimal or negligible. Estimates derived from water balance calculations by Goerner et al. (2009) and Dinka (2020) excluded direct flow of water to the lake from the irrigation practice in the nearby plantations as the main reason for the lake level rise and spatial expansion.

4.1. Conceptual model of the lake surface area expansion processes

We hypothesize that the increase in the surface area of the lake is driven by a combination of two processes: groundwater influx into the lake surface facilitated by active volcano-tectonic processes and volcano-tectonic-induced subsidence that creates favorable conditions for the water to expand to new areas. Detailed descriptions of the processes that gave rise to the lake surface area growth are provided below.

The Mount Fentale area is one of the most seismically active regions in the Ethiopian rift (Hunt et al., 2017). Ongoing volcanic and tectonic processes within and proximal to the mountain and the lake region reactivated existing structures as well as formed new ones, which can create new groundwater pathways or enhance existing ones that facilitate groundwater flow from the surrounding and deep aquifer systems to the lake. One manifestation of such process is the presence of hot springs at the current western and southwestern peripheries of the lake and those that are now submerged due to the lake expansion as noted in earlier studies (Goerner et al., 2009). Most of these hot springs in the study area (e.g., HS-I1 and HS-I2 in Fig. 2) as well as the MER in general are spatially aligned with the tectonic structures (Raggiunti et al., 2021). To the west and southwest of the lake, active NNE–SSW-oriented faults are believed to be the main channels for conveying groundwater to the lake. The continuity of the subsidence deformation signal proximal to the tectonic structures located to the northwest, west, and southwest of Lake Beseka (Fig. 7b) indicates the presence of active tectonic processes in the area. Potential reactivated processes in the nearby Mount Kone (see Fig. 1 for location), an area that has a history of occurrence of fissuring episodes as recent as less than 7000 years (Williams et al., 2004), could possibly have aided in reactivating the faults to the west and southwest of the lake. This is in contrast to the deformation signal of the area near the faults adjoining the lake on the eastern side (Fig. 7b). The temporal change in the physicochemical quality parameters of water samples from the lake (Section 3.4) and the dilution of the lake water with the addition of a new water type are spatially amplified near the western and southwestern edges of the lake (Fig. 2; Section 3.4) that are dominated by NNE–SSW-oriented faults. The fact that the groundwater flow direction of the watershed, a replica of the surface water flow direction (Fig. 2), is from west to east (Belay, 2009), explains the similarity of the water quality and isotopic parameters between the lake's western and northwestern escarpments (recharge zone), the springs, and the groundwater samples in the vicinity of the western and northwestern parts of the lake (Kebede et al., 2008). The analysis of the temperature of the lake water from the western and northwestern parts of the lake (~29 °C) in contrast to the eastern part (~24 °C) further demonstrates the influence of hot springs in altering the physical and chemical properties of the lake water (MWIE, 2015). This evidence further supports the claim of a role for active tectonic structures in the western and southwestern parts of the lake in injecting groundwater in the form of hot springs to the lake.

Asfaw (1982) credited the occurrence of a network of fissures to the north of Mount Fentale to an earthquake swarm that occurred between January and March 1981. Likewise, it is conceivable that seismic activities induced by active volcanic processes with epicenters proximal to the northern part of the lake region may be responsible for the formation of the network of fissures observed surrounding the foothills of Mount Fentale and Tinish Sabober (Figs. 7 and 8). Though not visible, such a process might also have formed fissures on the lake bottom surface that facilitated the transfer of groundwater to the lake surface and contributed to the lake surface area expansion. Though contrasting effects, similar processes of the development of ground cracks in the Lake Awassa watershed after repeated earthquake events were credited for the disappearance of small lakes and fluctuations experienced in Lake Awassa (Ayenew and Gebreegziabher, 2006). To the north of Lake Beseka, the high HCO_3^- concentrations observed in water samples from hot springs near the Mount Fentale area (Section 3.4) signify CO_2 contribution from the mantle source in clear contrast to the composition of the rainfall that is assumed to partly contribute to recharge of the regional groundwater system (Bretzler et al., 2011), and this indicates the connectivity of the aquifer systems with deep-seated active volcanic processes. This further consolidates the notion of the role of volcanic processes in the vicinity of the lake for the surface area growth. In addition, the higher LST values observed to the north of the lake (Fig. 8), the recurrence of seismic events (e.g., EP-1 and EP-2 in Figs. 7a and 7b), and the continuity of

the deformation signal (uplift as well as subsidence (Figs. 7a and 7b)) over time in concurrence to past observations (e.g., Asfaw et al., 2006), along with the episodical deformation rates (Figs. 7a and 7b; Section 3.2) near the caldera of Mount Fentale, indicate an ongoing active volcanic process (Lu and Dzurisin, 2014) that may lead (or have led) to the formation of a further network of fissures near the lake and/or underneath the lake/bottom. In a study conducted by MWIE (2014) on the lake level rise and potential design mitigation measures to reduce the impact, an increased discharge of groundwater was noted in the northern part of the lake, where the extensive fissure and fault networks prevail (Figs. 8 and 9).

Volcanic- and tectonic-induced high subsidence rates at the peripherals of the lake (Figs. 7a and 7b), particularly on the low-lying areas bordering the lake, are causing the elevation of the surface to become lower, thereby altering the existing elevation gradient (Fig. 2). With the addition of groundwater to the lake and the subsequent rise in the lake level, the water will be forced to follow the existing or new elevation gradient and to occupy new zones created by the subsidence process. For example, higher subsidence rates on the northern part of the lake (Fig. 7b) have led to the expansion of the lake in the direction of Tinish Sabober (Figs. 7a and 7b).

4.2. Future lake surface area expansion scenario

We combined the average elevation values of the lake surface obtained from the ALOS DEM in which we set the elevation of the lake surface (< 945 m) as a base measurement (shown in light yellow in Fig. 9) to highlight low-lying areas, the flow direction derived from the DEM (Fig. 2), and surface deformation rates calculated using the Sentinel-1 data (Fig. 7b) to consider future expansion scenarios and potential impacts. We anticipate that future expansion of the lake will be in the northwest, northeast, and south directions (Fig. 9). This is expected to affect the communities living in two major cities, particularly Metehara city because of the ongoing higher subsidence rates and because the city is situated at a lower elevation (Section 3.2). The western edges of Metehara city are slowly being encroached by the expanding lake, as can be seen from the historical growth of the lake surface area (1972–2020; Fig. 9). It is unfortunate that new homes are being built in this part of the city, as can be seen on recent google earth and Landsat 8 images.

The expansion of the lake had already submerged homes and infrastructure as well as forced the construction of new roads and railway lines to replace the affected infrastructure (MWIE, 2015). Future lake expansions are expected to affect infrastructure found in close proximity to the current boundary of the lake. For example, the road linking the Metehara and Addis Ketema cities (Fig. 9) is expected to be fully submerged in the coming years. The road lies in an area with low elevation values and experiences moderate subsidence rates (Fig. 7b); following the natural gradient flow of the area, it is expected that the lake growth will fully submerge the road. Likewise, the northern parts of Abadir farm (see Fig. 1 for its location) are expected to be impacted by the lake surface area growth (Fig. 9). Coupled with moderate rates of subsidence along the faults with the low-lying topography of the area, the newly established (after 2008 (Dinka, 2017)) Fentale irrigation scheme in the northwest edge of the study area (see Fig. 1 for location) is also impacted by the lake surface area expansion. The impact is expected to be much more pronounced in later years with progressive subsidence and lake surface area expansion, as revealed in Figs. 7b and 9. The saline lake water encroachment in these farms and other affected areas degrades the quality of the soil and adversely impacts productivity and/or the health of existing vegetation that will have profound repercussions on the ecosystem of the region unless proper mitigation measures are implemented soon. The true source of the groundwater attributed in this study as the primary cause of the lake expansion, whether from the regional water system or from the irrigation, requires further in-depth assessment to assist in the mitigation effort.

5. Study limitations

The lake level and surface area of Lake Beseka have increased dramatically over the past decades. Our study has no robust quantitative analysis of the water budget of the lake to provide more definitive answers to the causes of lake expansion. In this regard, this study has limitations. However, we analyzed multiple datasets and integrated existing information to narrow down the most probable causes of the lake surface area expansion. The chemical analysis of the lake water and hot springs indicated that groundwater influx occurred from adjacent areas to the lake. However, no data confirmed that the influx is increasing over time. Hot spring discharge data collected at three different times, assuming the bulk of the groundwater inflow comes from the springs, showed an irregular pattern. Discharge measurements of the hot springs in the area made in 1978 by Halcrow (1978) and in 2004 by Goerner et al. (2009) indicated consistent discharge rates of 0.05 m^3/s. On the contrary, the 1998 discharge rate measurement by Tessema (1998) showed a higher (1.2 m^3/s) discharge rate. Net groundwater flux to the lake system estimated through a conceptual water balance model developed by Dinka (2017) is in agreement with this rate. Considering evaporation (for example, Goerner et al., 2009 estimated 1.43 m^3/s of evaporation for 1989 when the size of the lake was approximately 35 km^2), loss of lake water via evaporation increases as surface area increases, these discharges are insignificant to cause the estimated lake expansion unless there are additional sources of water to the lake. We believe that groundwater influx into the lake surface facilitated by active volcano-tectonic processes and structures and ground subsidence that allowed more areas to be inundated by the lake water are the probable causes. The possible role of lake bottom morphological and deformation-induced changes on the latter requires close investigation. These could be accomplished through the multi-temporal acquisition and comparison of bathymetry data. Comparisons could be made between the two existing bathymetry maps produced in 1999 and 2004 to see possible changes (Belay, 2009; Goerner et al., 2009). However, the existing maps have a coarse vertical resolution (1–2 m) and hence may not be able to detect subtle elevation changes between the data acquisition times. We, therefore, recommend the multi-temporal acquisitions of high spatial resolution and accuracy bathymetry datasets to assess the possibility of lake bottom dynamics on the lake area expansion.

6. Conclusion

This study utilized multi-source remote sensing and relevant datasets to understand the causes of the lake surface area expansion of Lake Beseka from the perspective of volcano-tectonic processes. The following important conclusions have been drawn from this research:

1) The surface area of Lake Beseka is expanding at an alarming rate. The surface area calculated from satellite data showed an increase in area from 38.9 km^2 in 2001–52.1 km^2 in 2020.
2) The climate data analysis results indicate that climate has no contribution to the expansion of the surface area of Lake Beseka.
3) Satellite-based LST data showed thermal activity in areas to the north of this lake (at the foothills of an active volcano), which is potentially related to an active volcanic process.
4) Areas near the north, west, and southwest parts of the lake have experienced higher subsidence rates (up to −4.52 mm/yr), as demonstrated by the satellite SAR-based deformation analysis results, which is indicative of a potential active volcano-tectonic process in the study area.
5) The physicochemical and isotopic water quality analyses from previous studies revealed the addition of new sources of water to the lake. This supported the hypothesis that additional groundwater influx, which we believe is facilitated by the formation of new secondary porosities (e.g., fractures) resulting from ongoing volcano-tectonic processes, has contributed to the expansion of this lake.
6) Furthermore, ground deformation processes have created a conducive setting for the lake to expand and inundate new areas.

CRediT authorship contribution statement

Esayas Gebremichael: Conceptualization, Methodology, Formal analysis, Investigation, Resources, Data curation, Writing – original draft, Writing – review & editing, Visualization. **Wondwosen M. Seyoum:** Methodology, Formal analysis, Investigation, Writing – review & editing, Visualization. **Benite Ishimwe:** Writing – review & editing, Formal analysis, Visualization. **Guzalay Sataer:** Writing – review & editing, Resources.

Declaration of Competing Interest

The authors declare that they have no known competing financial interests or personal relationships that could have appeared to influence the work reported in this paper.

Acknowledgement

This research was supported by the Junior Faculty Summer Research Program at Texas Christian University.

Appendix A. Supporting information

Supplementary data associated with this article can be found in the online version at doi:10.1016/j.ejrh.2022.101093.

References

Acocella, V., Korme, T., Salvini, F., 2002. Formation of normal faults along the axial zone of the Ethiopian Rift. J. Struct. Geol. 25 (4) https://doi.org/10.1016/S0191-8141(02)00047-0.
Abbott, M.B., Anderson, L., 2009. Lake-level fluctuations. Encyclopedia of Earth Sciences Series. Springer, pp. 13–15.
Acocella, V., Abebe, B., Korme, T., 2011. Holocene opening directions along the axes of the Red Sea (Afar) and Main Ethiopian Rifts: An overview. Spec. Pap. Geol. Soc. Am. 478 (June), 25–35. https://doi.org/10.1130/2011.2478(02).
Alemayehu, T., Ayenew, T., Kebede, S., 2006. Hydrogeochemical and lake level changes in the Ethiopian Rift. J. Hydrol. 316 (1–4), 290–300. https://doi.org/10.1016/j.jhydrol.2005.04.024.
Asfaw, L.M., 1982. Development of earthquake-induced fissures in the Main Ethiopian Rift. Nature 297 (5865), 393–395. https://doi.org/10.1038/297393a0.
Asfaw, L.M., Beyene, H., Mkonnen, A., Oli, T., 2006. Vertical deformation in the Main Ethiopian Rift: Levelling results in its nothern part, 1995-2004. Geol. Soc. Spec. Publ. 259, 185–190. ⟨https://doi.org/10.1144/GSL.SP.2006.259.01.15⟩.
Ayenew, T., 2004. Environmental implications of changes in the levels of lakes in the Ethiopian Rift since 1970. Reg. Environ. Change 4 (4), 192–204. https://doi.org/10.1007/s10113-004-0083-x.
Ayenew, T., Gebreegziabher, Y., 2006. Application of a spreadsheet hydrological model for computing the long-term water balance of Lake Awassa, Ethiopia. Hydrol. Sci. J. 51 (3), 418–431. https://doi.org/10.1623/hysj.51.3.418.
Ayenew, T., Legesse, D., 2007. The changing face of the Ethiopian rift lakes and their environs: call of the time. Lakes Reserv.: Res. Manag. 12 (3), 149–165. https://doi.org/10.1111/j.1440-1770.2007.00332.x.
Ayenew, T., Kebede, S., Alemyahu, T., 2008. Environmental isotopes and hydrochemical study applied to surface water and groundwater interaction in the Awash River basin. Hydrol. Process. 22 (10) https://doi.org/10.1002/hyp.6716.
Balzter, H., 2001. Forest mapping and monitoring with interferometric synthetic aperture radar (InSAR). Prog. Phys. Geogr. 25 (2), 159–177. https://doi.org/10.1191/030913301666986397.

Barchi, M.R., Carboni, F., Michele, M., Ercoli, M., Giorgetti, C., Porreca, M., Chiaraluce, L., 2021. The influence of subsurface geology on the distribution of earthquakes during the 2016–2017 central Italy seismic sequence. Tectonophysics 807. https://doi.org/10.1016/j.tecto.2021.228797.
Barra, A., Solari, L., Béjar-Pizarro, M., Monserrat, O., Bianchini, S., Herrera, G., Moretti, S., 2017. A methodology to detect and update active deformation areas based on Sentinel-1 SAR images. Remote Sens. 9 (10) https://doi.org/10.3390/rs9101002.
Bartsch, A., Widhalm, B., Kuhry, P., Hugelius, G., Palmtag, J., Benjamin Siewert, M., 2016. Can C-band synthetic aperture radar be used to estimate soil organic carbon storage in tundra? Biogeosciences 13 (19), 5453–5470. https://doi.org/10.5194/bg-13-5453-2016.
Bekaert, D.P.S., Walters, R.J., Wright, T.J., Hooper, A., Parker, D.J., 2015. Statistical comparison of InSAR tropospheric correction techniques. Remote Sensing of Environment 170, 40–47. https://doi.org/10.1016/j.rse.2015.08.035.
Belay, E.A., 2009. Growing lake with growing problems: integrated hydrogeological investigation on Lake Beseka. Ethiopia. ⟨http://hss.ulb.uni-bonn.de/diss_online⟩.
Benvenuti, M., Carnicelli, S., Belluomini, G., Dainelli, N., Di Grazia, S., Ferrari, G.A., Kebede, S., 2002. The Ziway-Shala lake basin (main Ethiopian rift, Ethiopia): a revision of basin evolution with special reference to the Late Quaternary. J. Afr. Earth Sci. 35 (2) https://doi.org/10.1016/S0899-5362(02)00036-2.
Berhe, B.A., 2007. Brittle Fracture and Lake Level Change at Beseka: Main Ethiopian Rift, *Metehara Area*. Addis Ababa University.
Bilham, R., Bendick, R., Larson, K., Mohr, P., Braun, J., Tesfaye, S., Asfaw, L., 1999. Secular and tidal strain across the main ethiopian rift. Geophys. Res. Lett. 26 (18) https://doi.org/10.1029/1998GL005315.
Bonini, M., Corti, G., Innocenti, F., Manetti, P., Mazzarini, F., Abebe, T., Pecskay, Z., 2005. Evolution of the Main Ethiopian Rift in the frame of Afar and Kenya rifts propagation. Tectonics 24 (1), 1–21. https://doi.org/10.1029/2004TC001680.
Brehme, M., Giese, R., Suherlina, L., Kamah, Y., 2019. Geothermal sweetspots identified in a volcanic lake integrating bathymetry and fluid chemistry. Sci. Rep. 9 (1) https://doi.org/10.1038/s41598-019-52638-z.
Bretzler, A., Osenbrück, K., Gloaguen, R., Ruprecht, J.S., Kebede, S., Stadler, S., 2011. Groundwater origin and flow dynamics in active rift systems - A multi-isotope approach in the Main Ethiopian Rift. J. Hydrol. 402 (3–4), 274–289. https://doi.org/10.1016/j.jhydrol.2011.03.022.
Burgmann, R., Rosen, P.A., Fielding, E.J., 2000. Synthetic aperture radar interferometry to measure earth's surface topography and its deformation. Annu. Rev. Earth Planet. Sci. 28. https://doi.org/10.1146/annurev.earth.28.1.169.
Busker, T., Roo, A. de, Gelati, E., Schwatke, C., Adamovic, M., Bisselink, B., Cottam, A., 2019. A global lake and reservoir volume analysis using a surface water dataset and satellite altimetry. Hydrol. Earth Syst. Sci. 23 (2), 669–690.
Caputo, T., Sessa, E.B., Silvestri, M., Buongiorno, M.F., Musacchio, M., Sansivero, F., Vilardo, G., 2019. Surface temperature multiscale monitoring by thermal infrared satellite and ground images at campi flegrei volcanic area (Italy). Remote Sens. 11 (9) https://doi.org/10.3390/rs11091007.
Center for International Earth Science Information Network (CIESIN). (2018). Gridded Population of the World, Version 4 (GPWv4): Population Density, Revision 11. Palisades, NY: NASA Socioeconomic Data and Applications Center (SEDAC). Retrieved December 15, 2021, from (https://doi.org/https://doi.org/10.7927/H49C6VHW).
Chavez Hernandez, J.A., Lazecký, M., Šebesta, J., Bakoň, M., 2020. Relation between surface dynamics and remote sensor InSAR results over the Metropolitan Area of San Salvador. Nat. Hazards 103 (3). https://doi.org/10.1007/s11069-020-04150-1.
Chen, C.W., Zebker, H.A., 2001. Network approaches to two-dimensional phase unwrapping: intractability and two new algorithms: erratum. J. Opt. Soc. Am. A 18 (5), 1192. https://doi.org/10.1364/josaa.18.001192.
Chen, Y., Zhang, G., Ding, X., Li, Z., 2000. Monitoring earth surface deformations with InSAR technology: principles and some critical issues. J. Geospatial Eng. 2 (1), 3–22.
Chernet, T., Hart, W.K., Aronson, J.L., Walter, R.C., 1998. New age constraints on the timing of volcanism and tectonism in the northern Main Ethiopian Rift - southern Afar transition zone (Ethiopia). J. Volcanol. Geotherm. Res. 80 (3–4) https://doi.org/10.1016/S0377-0273(97)00035-8.
Crosetto, M., Monserrat, O., Cuevas-González, M., Devanthéry, N., Crippa, B., 2016. Persistent Scatterer Interferometry: a review. ISPRS J. Photogramm. Remote Sens. Vol. 115, 78–89. https://doi.org/10.1016/j.isprsjprs.2015.10.011.
Darge, Y.M., Hailu, B.T., Muluneh, A.A., Kidane, T., 2019. Detection of geothermal anomalies using Landsat 8 TIRS data in Tulu Moye geothermal prospect, Main Ethiopian Rift. Int. J. Appl. Earth Obs. Geoinf. 74, 16–26. https://doi.org/10.1016/j.jag.2018.08.027.
Dershaye, B., 2017. Environmental Impact Analysis of Infrastructures Development and Lake Beseka Expansion on the Integrity of Fentale-Metehara Blister Caves in the Main Ethiopian Rift. Addis Ababa University.
Megersa Olumana Dinka Analyzing the extents of Basaka Lake expansion and soil and water quality status of Matahara irrigation scheme, Awash Basin (Ethiopia) Dissertation 2010.https://inis.iaea.org/search/searchsinglerecord.aspx?recordsFor=SingleRecord&RN=43074757.
Dinka, M.O., 2012. Analysing the extent (size and shape) of Lake Basaka expansion (Main Ethiopian Rift Valley) using remote sensing and GIS. Lakes Reserv.: Res. Manag. 17 (2), 131–141. https://doi.org/10.1111/j.1440-1770.2012.00500.x.
Dinka, Megersa Olumana, 2017. Analysing the temporal water quality dynamics of Lake Basaka, Central Rift Valley of Ethiopia. IOP Conf. Ser. Earth Environ. Sci. 52 (1) https://doi.org/10.1088/1742-6596/52/1/012057.
Dinka, Megersa Olumana, 2020. Estimation of groundwater contribution to Lake Basaka in different hydrologic years using conceptual netgroundwater flux model. J. Hydrol.: Reg. Stud. 30. https://doi.org/10.1016/j.ejrh.2020.100696.
Ethiopian Institute of Geological Surveys), M. of M. and E. EIGS, 1978. Geological Map of the Nazret Sheet _NC37-15., scale 1:250,000. Ethiopia, Addis Ababa.
Kendall, M.G., 1975. Rank Correlation Methods. Griffin, London.
Lu, Z., Dzurisin, D., 2014. InSAR Imaging of Aleutian Volcanoes. Springer Berlin Heidelberg.
Lyon, T.J., Filmer, M.S., Featherstone, W.E., 2018. On the use of repeat leveling for the determination of vertical land motion: artifacts, aliasing, and extrapolation errors. J. Geophys. Res. Solid Earth 123 (8), 7021–7039. https://doi.org/10.1029/2018JB015705.
Ma, J., Chen, S., Hu, X., Liu, P., Liu, L., 2010. Spatial-temporal variation of the land surface temperature field and present-day tectonic activity. Geosci. Front. 1 (1), 57–67. https://doi.org/10.1016/j.gsf.2010.09.002.
Ministry of Water Irrigation and Electricity, T.F.D.R. of E. MWIE, 2014. Assessment. and Evaluation of the Causes for Beseka Lake Level Rise and Designing Mitigation Measures Part II: Study for Medium-and Long-Term Solutions, Main Report. Addis Ababa, Ethiopia.
Foumelis, M., Blasco, J.M. D., Desnos, Y.L., Engdahl, M., Fernández, D., Veci, L., … Wong, C. (2018). ESA SNAP - Stamps integrated processing for Sentinel-1 persistent scatterer interferometry. International Geoscience and Remote Sensing Symposium (IGARSS), 2018-July, 1364–1367. ⟨https://doi.org/10.1109/IGARSS.2018.8519545⟩.
Fubelli, G., Dramis, F. (2015). Geo-hazard in Ethiopia. In World Geomorphological Landscapes (pp. 351–367). https://doi.org/10.1007/978–94-017–8026-1_20.
Funk, C., Peterson, P., Landsfeld, M., Pedreros, D., Verdin, J., Shukla, S., Michaelsen, J., 2015. The climate hazards infrared precipitation with stations - a new environmental record for monitoring extremes. Sci. Data 2, 1–21. https://doi.org/10.1038/sdata.2015.66.
Fiaschi, S., Holohan, E.P., Sheehy, M., Floris, M., 2019. PS-InSAR analysis of Sentinel-1 data for detecting ground motion in temperate oceanic climate zones: A case study in the Republic of Ireland. Remote Sensing 11 (3), 348. https://doi.org/10.3390/rs11030348.
Funk, C.C., Peterson, P.J., Landsfeld, M.F., Pedreros, D.H., Verdin, J.P., Rowland, J.D., Verdin, A.P., 2014. A quasi-global precipitation time series for drought monitoring. U. S. Geol. Surv. Data Ser. 832, 4.
Gama, F.F., Mura, J.C., Paradella, W.R., de Oliveira, C.G., 2020. Deformations prior to the brumadinho dam collapse revealed by sentinel-1 insar data using sbas and psi techniques. Remote Sens. 12 (21) https://doi.org/10.3390/rs12213664.
Gasse, E., Street, F.A., 1978. Late Quaternary Lake-level fluctuations and environments of the northern Rift valley and Afar region (Ethiopia and Djibouti). Palaeogeogr. Palaeoclimatol. Palaeoecol. 24 (4) https://doi.org/10.1016/0031-0182(78)90011-1.
Gebremichael, E., Sultan, M., Becker, R., El Bastawesy, M., Cherif, O., Emil, M., 2018. Assessing land deformation and sea encroachment in the nile delta: a radar interferometric and inundation modeling approach. J. Geophys. Res.: Solid Earth 123 (4), 3208–3224. https://doi.org/10.1002/2017JB015084.
Goerner, A., Jolie, E., Gloaguen, R., 2009. Non-climatic growth of the saline Lake Beseka, Main Ethiopian Rift. J. Arid Environ. 73 (3), 287–295. https://doi.org/10.1016/j.jaridenv.2008.09.015.

Halcrow, W., 1978. The study of Beseka Lake levels. In The Study of Beseka Lake Levels. Report for the Government of Ethiopia. Awash Valley Development Agency, San Bernardino, CA, p. 83.
Haley, M., Ahmed, M., Gebremichael, E., Murgulet, D., Starek, M., 2022. Land subsidence in the texas coastal bend: locations, rates, triggers, and consequences. Remote Sens. 14 (1).
Hancock, P.L., Chalmers, R.M.L., Altunel, E., Çakir, Z., 1999. Travitonics: using travertines in active fault studies. J. Struct. Geol. 21 (8–9), 903–916. https://doi.org/10.1016/S0191-8141(99)00061-9.
Hanssen, R.F., 2001. Radar interferometry: data interpretation and error analysis, 2. Springer Science & Business Media.
Harris, W.C., 1844. The Highlands of Ethiopia, 3. J. Winchester, New World Press.
Hayes, P., Jones, E.S., Stadler, T.J., Barnhart, W.D., McNamara, D.E., Benz, H.M., … Villaseñor, A. (2014). Seismicity of the Earth 1900–2013. East African Rift. In Open-File Report 2010–1083-P (Vol. 1258). https://doi.org/10.3133/ofr20101083P.
Hooper, A., Segall, P., Zebker, H., 2007. Persistent scatterer interferometric synthetic aperture radar for crustal deformation analysis, with application to Volcán Alcedo, Galápagos. J. Geophys. Res. Solid Earth 112 (7). https://doi.org/10.1029/2006JB004763.
Hooper, Andrew. (2010). A statistical-cost approach to unwrapping the phase of InSAR time series. Proceeding of International Workshop on ERS SAR, 2009(March), 1–5. Retrieved from ⟨http://radar.tudelft.nl/~ahooper/Hooper_FRINGE_2009.pdf⟩.
Hooper, A., Zebker, H., Segall, P., Kampes, B., 2004. A new method for measuring deformation on volcanoes and other natural terrains using InSAR persistent scatterers. Geophys. Res. Lett. 31 (23), 1–5. https://doi.org/10.1029/2004GL021737.
Hooper, A., Bekaert, D., Spaans, K., Arikan, M., 2012. Recent advances in SAR interferometry time series analysis for measuring crustal deformation. Tectonophysics 514–517, 1–13. https://doi.org/10.1016/j.tecto.2011.10.013.
Hunt, J.A., Zafu, A., Mather, T.A., Pyle, D.M., Barry, P.H., 2017. Spatially Variable CO2 Degassing in the Main Ethiopian Rift: Implications for Magma Storage, Volatile Transport, and Rift-Related Emissions. Geochemistry, Geophysics, Geosystems 18 (10), 3714–3737. https://doi.org/10.1002/2017GC006975.
Hutchison, W., Biggs, J., Mather, T.A., Pyle, D.M., Lewi, E., Yirgu, G., Fischer, T.P., 2016. Causes of unrest at silicic calderas in the East African Rift: new constraints from InSAR and soil-gas chemistry at Aluto volcano, Ethiopia. Geochem., Geophys., Geosyst. 17 (8), 3008–3030.
Jia, H., Liu, L., 2016. A technical review on persistent scatterer interferometry. J. Mod. Transp. Vol. 24, 153–158. https://doi.org/10.1007/s40534-016-0108-4.
Jimenez-Munoz, J.C., Cristobal, J., Sobrino, J.A., Sòria, G., Ninyerola, M., Pons, X., 2009. Revision of the single-channel algorithm for land surface temperature retrieval from landsat thermal-infrared data. IEEE Trans. Geosci. Remote Sens. 47 (1), 339–349. https://doi.org/10.1109/TGRS.2008.2007125.
Jin, L., Whitehead, P.G., Bussi, G., Hirpa, F., Taye, M.T., Abebe, Y., Charles, K., 2021. Natural and anthropogenic sources of salinity in the Awash River and Lake Beseka (Ethiopia): modelling impacts of climate change and lake-river interactions. J. Hydrol. Reg. Stud. 36. https://doi.org/10.1016/j.ejrh.2021.100865.
Kampes, B., Usai, S. (1999). Doris: The delft object-oriented radar interferometric software. 2nd International Symposium on Operationalization of Remote Sensing, Enschede, the Netherlands, 16, 20.
Kebede, E., Mariam, Z.G., Ahlgren, I., 1994. The Ethiopian Rift Valley lakes: chemical characteristics of a salinity-alkalinity series. Hydrobiologia 288 (1), 1–12. https://doi.org/10.1007/BF00006801.
Kapchenko, L.N., Grozdova, T.P., 1997. On the origin of Lake Baikal water. Water Resources 24 (5), 589–595.
Kebede, G., 1987. Hydrogeology of Nazreth area, NC 37-15. Addis Ababa, Ethiopia.
Kebede, S., Travi, Y., Asrat, A., Alemayehu, T., Ayenew, T., Tessema, Z., 2008. Groundwater origin and flow along selected transects in Ethiopian rift volcanic aquifers. Hydrogeology Journal 16 (1), 55–73. https://doi.org/10.1007/s10040-007-0210-0.
Keir, D., Ebinger, C.J., Stuart, G.W., Daly, E., Ayele, A., 2006. Strain accommodation by magmatism and faulting as rifting proceeds to breakup: Seismicity of the northern Ethiopian rift. J. Geophys. Res. Solid Earth 111 (5). https://doi.org/10.1029/2005JB003748.
Keir, D., Stuart, G.W., Jackson, A., Ayele, A., 2006. Local earthquake magnitude scale and seismicity rate for the Ethiopian rift. Bull. Seismol. Soc. Am. 96 (6), 2221–2230. https://doi.org/10.1785/0120060051.
Klemperer, S.L., Cash, M.D., 2007. Temporal geochemical variation in Ethiopian Lakes Shala, Arenguade, Awasa, and Beseka: Possible environmental impacts from underwater and borehole detonations. J. Afr. Earth Sci. 48 (2–3), 174–198.
Kraemer, B.M., Seimon, A., Adrian, R., McIntyre, P.B., 2020. Worldwide lake level trends and responses to background climate variation. Hydrol. Earth Syst. Sci. 24 (5), 2593–2608. https://doi.org/10.5194/hess-24-2593-2020.
Kucharski, D., Kirchner, G., Koidl, F., Fan, C., Carman, R., Moore, C., Feng, Q., 2014. Attitude and spin period of space debris envisat measured by satellite laser ranging. IEEE Trans. Geosci. Remote Sens. 52 (12), 7651–7657. https://doi.org/10.1109/TGRS.2014.2316138.
Latip, A.S. A., Matori, A., Aobpaet, A., & Din, A.H. M. (2015). Monitoring of offshore platform deformation with stanford method of Persistent Scatterer (StaMPS). International Conference on Space Science and Communication, IconSpace, 2015-Septe, 79–83. ⟨https://doi.org/10.1109/IconSpace.2015.7283785⟩.
Le Turdu, C., Tiercelin, J.J., Gibert, E., Travi, Y., Lezzar, K.E., Richert, J.P., Taieb, M., 1999. The Ziway-Shala lake basin system, Main Ethiopian Rift: influence of volcanism, tectonics, and climatic forcing on basin formation and sedimentation. Palaeogeogr., Palaeoclimatol., Palaeoecol. 150 (3–4), 135–177. https://doi.org/10.1016/S0031-0182(98)00220-X.
Mann, H.B. (1945). Non-Parametric Test Against Trend. *Econometrica*, 13(3), 245–259. Retrieved from ⟨http://www.economist.com/node/18330371?story%7B_%7Did=18330371⟩.
Mohr, P., 1987. Patterns of faulting in the Ethiopian rift valley. Tectonophysics 143 (1–3). https://doi.org/10.1016/0040-1951(87)90086-2.
Mulugeta, S., Fedler, C., Ayana, M., 2019. Analysis of long-term trends of annual and seasonal rainfall in the Awash River Basin, Ethiopia. Water (Switz.) 11 (7). https://doi.org/10.3390/w11071498.
Ministry of Water Irrigation and Electricity, T.F. D.R. of E., (MWIE). (2015). *The Project for Groundwater Assessment in the Middle Awash River Basin in the Federal Democratic Republic of Ethiopia*. Retrieved from ⟨https://openjicareport.jica.go.jp/pdf/12248605.pdf⟩.
Owen, R.B., Renaut, R.W., Muiruri, V.M., Rabideaux, N.M., Lowenstein, T.K., McNulty, E.P., Stockhecke, M., 2019O. Quaternary history of the Lake Magadi Basin, southern Kenya Rift: Tectonic and climatic controls. Palaeogeogr. Palaeoclimatol. Palaeoecol. 518. https://doi.org/10.1016/j.palaeo.2019.01.017.
Parastatidis, D., Mitraka, Z., Chrysoulakis, N., Abrams, M., 2017. Online global land surface temperature estimation from landsat. Remote Sensing 9 (12), 1208.
Pepe, A., Calò, F., 2017. A review of interferometric synthetic aperture RADAR (InSAR) multi-track approaches for the retrieval of Earth's Surface displacements. Appl. Sci. 7 https://doi.org/10.3390/app7121264.
Poland, M., Bürgmann, R., Dzurisin, D., Lisowski, M., Masterlark, T., Owen, S., Fink, J., 2006. Constraints on the mechanism of long-term, steady subsidence at Medicine Lake volcano, northern California, from GPS, leveling, and InSAR. J. Volcanol. Geotherm. Res. 150 (1–3), 55–78. https://doi.org/10.1016/j.jvolgeores.2005.07.007.
Prange, M., Wilke, T., Wesselingh, F.P., 2020. The other side of sea level change. Commun. Earth Environ. 1 (1) https://doi.org/10.1038/s43247-020-00075-6.
Raggiunti, M., Keir, D., Pagli, C., 2021. Mapping hydrothermal alteration at the fentale-dofan magmatic segment of the main ethiopian rift. Front. Earth Sci. 9. https://doi.org/10.3389/feart.2021.716144.
Sakai, H., Fujii, R., Sugimoto, M., Setoguchi, R., Paudel, M.R., 2016. Two times lowering of lake water at around 48 and 38 ka, caused by possible earthquakes, recorded in the Paleo-Kathmandu lake, central Nepal Himalaya. Earth Planets Space 68 (1). https://doi.org/10.1186/s40623-016-0413-5.
Sekertekin, A., Bonafoni, S., 2020. Land surface temperature retrieval from Landsat 5, 7, and 8 over rural areas: Assessment of different retrieval algorithms and emissivity models and toolbox implementation. Remote Sens. 12 (2) https://doi.org/10.3390/rs12020294.
Sen, P.K., 1968. Estimates of the regression coefficient based on Kendall's tau. J. Am. Stat. Assoc. 63 (324), 1379–1389. https://doi.org/10.1080/01621459.1968.10480934.
Seyoum, W.M., Milewski, A.M., Durham, M.C., 2015. Understanding the relative impacts of natural processes and human activities on the hydrology of the Central Rift Valley lakes, East Africa. Hydrol. Process. 29 (19), 4312–4324. https://doi.org/10.1002/hyp.10490.
Sousa, J.J., Hooper, A.J., Hanssen, R.F., Bastos, L.C., 2010. Comparative Study of Two Different PS-InSAR Approaches: DePSI vs. StaMPS, 677. ESA Special Publication, p. 72.

Talbot, M.R., 2005. In: Selley, R.C., Cocks, L.R.M., Plimer, I.R. (Eds.), Sedimentary Environments | Lake Processes and Deposits. Encyclopedia of Geology, pp. 550–561. https://doi.org/10.1016/B0-12-369396-9/00493-7.

Tantianuparp, P., Shi, X., Zhang, L., Balz, T., Liao, M., 2013. Characterization of landslide deformations in three Gorges area using multiple inSAR data stacks. Remote Sens. 5 (6) https://doi.org/10.3390/rs5062704.

Temtime, T., Biggs, J., Lewi, E., Ayele, A., 2020. Evidence for active rhyolitic dike intrusion in the northern main ethiopian rift from the 2015 fentale seismic swarm. Geochem. Geophys. Geosyst. 21 (6) https://doi.org/10.1029/2019GC008550.

Tessema, Z. (1998). Hydrochemical and water balance approach in the study of high water level rise of Lake Beseka. Unpublished M. Sc thesis, University of Birmingham, UK, 90pp.

Theuerkauf, E.J., Braun, K.N., 2021. Rapid water level rise drives unprecedented coastal habitat loss along the Great Lakes of North America. J. Gt. Lakes Res. 47 (4) https://doi.org/10.1016/j.jglr.2021.05.004.

United States Geological Survey (USGS). (2020). What are the band designations for the Landsat satellites? Retrieved November 24, 2021, from ⟨https://www.usgs.gov/faqs/what-are-band-designations-landsat-satellites?qt-news_science_products=0#qt-news_science_products⟩.

Vallet-Coulomb, C., Gasse, F., Sonzogni, C., 2008. Seasonal evolution of the isotopic composition of atmospheric water vapour above a tropical lake: deuterium excess and implication for water recycling. Geochim. Et. Cosmochim. Acta 72 (19), 4661–4674. https://doi.org/10.1016/j.gca.2008.06.025.

Wang, J., Song, C., Reager, J.T., Yao, F., Famiglietti, J.S., Sheng, Y., Wada, Y., 2018. Recent global decline in endorheic basin water storages. Nat. Geosci. 11 (12), 926–932. https://doi.org/10.1038/s41561-018-0265-7.

Wauthier, C., Cayol, V., Kervyn, F., D'Oreye, N., 2012. Magma sources involved in the 2002 Nyiragongo eruption, as inferred from an InSAR analysis. J. Geophys. Res. Solid Earth 117 (5). https://doi.org/10.1029/2011JB008257.

White, R., McCausland, W., 2016. Volcano-tectonic earthquakes: a new tool for estimating intrusive volumes and forecasting eruptions. J. Volcanol. Geotherm. Res. 309, 139–155. https://doi.org/10.1016/j.jvolgeores.2015.10.020.

Williams, F.M., Williams, M.A.J., Aumento, F., 2004. Tensional fissures and crustal extension rates in the northern part of the Main Ethiopian Rift. J. Afr. Earth Sci. 38 (2), 183–197. https://doi.org/10.1016/j.jafrearsci.2003.10.007.

World Bank. (2021). Population density (people per sq. km of land area) - Ethiopia | Data. Retrieved December 29, 2021, from ⟨https://data.worldbank.org/indicator/EN.POP.DNST?locations=ET⟩.

Wurtsbaugh, W.A., Miller, C., Null, S.E., Justin De Rose, R., Wilcock, P., Hahnenberger, M., Moore, J., 2017. Decline of the world's saline lakes. Nat. Geosci. 10 (11), 816–821. https://doi.org/10.1038/NGEO3052.

Yang, K., Yan, L., Huang, G., Chen, C., Wu, Z., 2016. Monitoring building deformation with InSAR: experiments and validation. Sens. (Switz.) 16 (12). https://doi.org/10.3390/s16122182.

Yimer, Y.A., Jin, L., 2020. Impact of Lake Beseka on the Water Quality of Awash River, Ethiopia. American Journal of Water Resources 8 (1), 21–30. https://doi.org/10.12691/ajwr-8-1-3.

Zebker, H.A., Villasenor, J., 1992. Decorrelation in interferometric radar echoes. IEEE Trans. Geosci. Remote Sens. 30 (5), 950–959. https://doi.org/10.1109/36.175330.

Zuhlke, M., Fomferra, N., Brockmann, C., Peters, M., Veci, L., Malik, J., Regner, P. (2015). SNAP (Sentinel Application Platform) and the ESA Sentinel 3 Toolbox. In Sentinel-3 for Science Workshop, Proceedings of a workshop held 2–5 June, 2015 in Venice, Italy (Vol. 12, p. 21). Retrieved from ⟨http://adsabs.harvard.edu/abs/2015ESASP.734E.21Z⟩.